Effects of wave-current interaction on rip currents

Jie Yu[1]
Department of Ocean Engineering, Florida Atlantic University, Boca Raton, Florida, USA

Donald N. Slinn
Department of Civil and Coastal Engineering, University of Florida, Gainesville, Florida, USA

Received 16 August 2001; revised 15 February 2002; accepted 11 June 2002; published 20 March 2003.

[1] The time evolution of rip currents in the nearshore is studied by numerical experiments. The generation of rip currents is due to waves propagating and breaking over alongshore variable topography. Our main focus is to examine the significance of wave-current interaction as it affects the subsequent development of the currents, in particular when the currents are weak compared to the wave speed. We describe the dynamics of currents using the shallow water equations with linear bottom friction and wave forcing parameterized utilizing the radiation stress concept. The slow variations of the wave field, in terms of local wave number, frequency, and energy (wave amplitude), are described using the ray theory with the inclusion of energy dissipation due to breaking. The results show that the offshore directed rip currents interact with the incident waves to produce a negative feedback on the wave forcing, hence to reduce the strength and offshore extent of the currents. In particular, this feedback effect supersedes the bottom friction such that the circulation patterns become less sensitive to a change of the bottom friction parameterization. The two physical processes arising from refraction by currents, bending of wave rays and changes of wave energy, are both found to be important. The onset of instabilities of circulations occurs at the nearshore region where rips are "fed," rather than offshore at rip heads as predicted with no wave-current interaction. The unsteady flows are characterized by vortex shedding, pairing, and offshore migration. Instabilities are sensitive to the angle of wave incidence and the spacing of rip channels. *INDEX TERMS:* 4546 Oceanography: Physical: Nearshore processes; 4560 Oceanography: Physical: Surface waves and tides (1255); 4255 Oceanography: General: Numerical modeling; 4512 Oceanography: Physical: Currents; *KEYWORDS:* rip currents, wave breaking, wave radiation stress, wave-current interaction

Citation: Yu, J., and D. N. Slinn, Effects of wave-current interaction on rip currents, *J. Geophys. Res.*, *108*(C3), 3088, doi:10.1029/2001JC001105, 2003.

1. Introduction

[2] When surface waves break on a beach, wave energy is lost to turbulence generated in the process of breaking, and wave momentum is transferred into the water column generating nearshore currents. There are two current systems whose flow structures are predominantly horizontal, alongshore currents caused by obliquely incident waves and cell-like circulations, which can occur when waves are nearly at normal incidence. Often described as narrow, jet-like, and seaward directed flows, rip currents are part of these cellular circulations, "fed" by the converging alongshore flows close to the shoreline. Rip currents can cause a seaward transport of beach sand, hence have direct impacts on beach morphology. On the other hand, the circulations may produce sufficient exchange of nearshore and offshore water, thus provide a flush of the nearshore region affecting the across-shore mixing of heat, nutrients, chemical, and biological species.

[3] Observations on the occurrence of rip currents, the associated sediment transport and subsequent shoreline evolution are many, including *Shepard et al.* [1941], *Shepard and Inman* [1950, 1951], *Cooke* [1970], and *Smith and Largier* [1995] in southern California, *McKenzie* [1958] and *Short* [1984, 1985] in Australia, *Harris* [1961, 1964] in South Africa, *Sonu* [1972] in Florida, *Hunter et al.* [1979] in southern Oregon, and *Sasaki and Horikawa* [1979] in Japan. Some of the beaches studied were alongshore variable, with rip currents located at rip channels (bottom depressions oriented primarily across-shore). Other beaches, however, were practically alongshore uniform.

[4] Even in the earliest investigations [e.g., *Shepard et al.*, 1941; *Shepard and Inman*, 1950, 1951], it was already recognized that the alongshore variation in the surface wave

[1] Now at Division of Earth and Ocean Sciences, Duke University, Durham, North Carolina, USA.

0148-0227/03/2001JC001105$09.00

field is important to the generation of rip currents. It is known that propagating surface waves produce a mass transport in the direction of wave propagation, which is a second-order correction to the linear wave theory and arises from the nonlinearity. When waves encounter a beach and break, water will pile up onshore, leading to a slight increase of the mean water surface level (set-up) toward the shoreline. This provides a pressure gradient to drive a seaward directed flow, returning water brought onshore by waves. If both beach and waves are uniform alongshore, this returning current is expected to be so too. Furthermore, if the waves are normally incident, alongshore flows are not generated. A two dimensional physical picture is then produced in the vertical plane across-shore, including a longshore uniform wave set-up, and a vertical circulation formed between the onshore wave induced mass drift and the returning current such that at the steady state the net transport of water across-shore is zero. This returning current may have various kinds of vertical structures, depending on the conditions of waves and beaches. For instance, it may be strongly concentrated near the seabed, appearing as the so-called undertow, or possibly be distributed over the intermediate depths so as to balance the onshore mass drifts in the surface and bottom boundary layers [*Longuet-Higgins*, 1953]. On the other hand, if alongshore variation is introduced to the wave field, the wave set-up will no longer be alongshore uniform. The resulting pressure gradients will drive alongshore flows toward regions of low set-up (i.e., low pressure), leading to horizontal circulations with offshore flows concentrated in regions of low set-up and onshore flows in between.

[5] This physical picture of horizontal circulations was first depicted quantitatively by *Bowen* [1969b]. He described the structure of cellular circulations produced by a normally incident wave train which has an assumed alongshore variation in the wave height, using two dimensional shallow water equations. The essence of the theory is the use of (1) radiation stress which represents the excess flux of momentum due to the presence of waves, (2) empirical knowledge of breaking wave height, and (3) assumptions on the forms of friction mechanisms which can be bottom friction, and/or lateral mixing due to turbulence. The concept of radiation stress was developed for small amplitude waves in irrotational flows, in a series of papers by *Longuet-Higgins and Stewart* [1960, 1961, 1962, 1964]. Extrapolation of the concept to breaking waves in the surf zone has been done since [*Bowen*, 1969a; *Longuet-Higgins*, 1970; *Thornton*, 1970]. (Though not well justified, this type of formulation has been used in studies of alongshore currents. By tuning the free parameters, such as coefficients of bottom friction and lateral mixing, reasonable comparisons with observations, particularly on plane beaches, have been achieved.) Using similar approaches, a number of studies were subsequently developed to explore different mechanisms which might produce the necessary alongshore variability on the wave field which had simply been assumed by Bowen. In the presence of longshore variable topography, this can be introduced by taking into account wave refraction (and perhaps wave diffraction) due to the topography [e.g., *Noda*, 1974; *Liu and Mei*, 1976]. These studies have generally ignored the effects of currents on waves, assuming it to be negligible because of weak currents. Nonlinear convective inertia, which is important to produce narrow offshore flows [*Arthur*, 1962; *Bowen*, 1969b], was also not considered in some of the studies. While most observations of rip currents are on alongshore variable beaches, studies of rip currents on alongshore uniform beaches indicated that alongshore variability in the wave field may also be introduced by interaction between incident waves and synchronized edge waves [*Bowen and Inman*, 1969], between two incident wave trains of the same frequency [*Dalrymple*, 1975], by instabilities involving the deformation of the erodible seabed [*Hino*, 1974] or by instabilities arising from the interaction of waves and the circulating currents [*LeBlond and Tang*, 1974; *Dalrymple and Lozano*, 1978; *Miller and Barcilon*, 1978; *Falqués et al.*, 1999]. These studies have also generally neglected the nonlinear convective inertia terms, and the effect of currents on waves, except in these last mentioned studies which show that cellular circulations can be initiated if the mutual interaction of waves and currents is accounted for. This suggests that the interaction can be of importance even when the currents are weak. Comparing their results with those of *Bowen* [1969b], *LeBlond and Tang* [1974] pointed out that wave-current interaction tends to reduce the strength of rip currents. Observations [*Harris*, 1967; *Arthur*, 1950] also show that wave refraction due to rip currents can be strong.

[6] Recently, *Haas et al.* [1998] reported a numerical simulation of a laboratory rip current system. The experiments [*Haller et al.*, 1997] were conducted in a wave basin (20 m $\times$ 20 m) with a barred beach. Two narrow rip channels, 1.8 m wide each, were cut transversely across the bar. Waves were normally incident. In the numerical model, the currents were described by the two dimensional shallow water equations with forcing due to wave breaking, and the wave equations are quasi steady. They found that the offshore extent of rip currents can be significantly reduced if the effects of currents on waves are considered. A clear physical explanation was not given, though they did notice the slight change of the wave height in rip channels when the interaction is included. The rip channels are sharp edged, and their width is comparable to the local water wavelength. This indicates that both the topography and currents may have spatial variations on the scale comparable or less than the water wavelength, implying significant diffractive effects. Simulations for the same laboratory set up were made later by *Chen et al.* [1999] using the extended Boussinesq equations [*Wei et al.*, 1995]. Such modeling resolves the wave motion and the induced currents together, therefore always accounts for the mutual interaction. It is thus not possible to compare results with and without interaction. *Chen et al.* [1999] indeed observed strong wave diffraction. The rip currents were found to be unstable. *Haas et al.* [1998] also mentioned this, but did not give details.

[7] This paper is aimed at improving our understanding of the physical processes involved in the wave-current interaction as it affects the subsequent development of rip currents. Attention will be on rip currents driven by topography to avoid the uncertainty of formation mechanisms of rip currents on alongshore uniform beaches. We are particularly interested to find out if the weak currents generated by a gentle alongshore variation in the wave

field, as in many previous studies, can cause significant refractive effect on the waves so as to change the structure of the forcing which drives the currents. In addition, we wish to address some issues which have not been considered sufficiently, such as the effect of the interaction on the development of instabilities of the cellular circulations, the dependence of the flow on physical parameters, for example, the wave height, the angle of wave incidence, rip channel spacing and depth, etc. We shall restrict ourselves to the study of an idealized system which isolates the main physical features from some others which, though possibly of importance in real oceanic processes, seem peripheral to our purpose here. Because of this, detailed comparison with observations, without the inclusion of some more realistic features, would need cautious interpretation and is placed beyond the scope of this study.

[8] The outline of the paper is as follows. The formulation of the problem and numerical procedure are described in section 2. Results from numerical experiments are presented in section 3. The results with and without wave-current interaction are first compared to demonstrate the significant difference. An explanation of the causes of such changes is then given. The basic features of rip currents and the nature of unsteady turbulent rip currents are discussed. Conclusions from the numerical experiments are given in section 4, followed by a few remarks on the limitations of the model and possible future improvements.

2. Formulation

[9] The basic beach bathymetry is alongshore uniform with a shore parallel bar located 80 meters from the shoreline. A gentle sinusoidal perturbation is then added at the bar to produce the necessary alongshore variability; see Figure 1. The mathematical description of the topography is given in Appendix A. Here x is the across-shore coordinate, pointing seaward, y is in the alongshore direction. ϵ and λ are, respectively, the magnitude and wavelength of the perturbation. In other words, ϵ measures the depth of rip channels (i.e., the transverse bar troughs), and λ measures the channel spacing and the channel width as well. Without the perturbation, the alongshore uniform bathymetry is essentially the alongshore average of the topography measured at Duck, North Carolina [*Lippmann et al.*, 1999]. This does not imply an attempt to simulate a situation at Duck, but is merely to represent a barred beach. The sinusoidal form of the perturbation is chosen for convenience, but as will be seen in section 3.1, it demonstrates clearly the importance of nonlinear convective inertia on narrowing the offshore flows.

[10] As is commonly done in modeling nearshore currents, we utilize two dimensional shallow water equations to describe the depth averaged and time averaged (with respect to the period of incident waves) mean flows. Due to the time averaging, the effects of rapidly varying wave motions appear as the forcing terms in the momentum balance of the slowly varying currents. These are similar to the Reynolds stress terms for turbulent flows. Bottom friction arises from the depth integration and appears as a body force to dissipate the energy of the currents. As by *Allen et al.* [1996], we use a linear bottom friction model. This is justifiable in the present study because the rip currents are expected to be weak due to the gentle topography variation. On the other hand, previous studies [e.g., *Özkan-Haller and Kirby*, 1999; *Thornton and Guza*, 1986] show that a linear bottom friction model is able to produce reasonable results even when currents are strong and a nonlinear model is expected, theoretically, to be more appropriate. Effects due to different formulations of bottom friction are not the subject of this study. Lateral mixing, due to turbulence at small scales and possibly the dispersive effect of the vertical fluctuation in the velocities of currents [*Svendsen and Putrevu*, 1994], can be important in real oceanic processes. Nevertheless, we shall neglect this effect in this idealized system to avoid additional uncertain parameterization. We shall also use a rigid lid approximation to the mean water surface to avoid numerical complications in dealing with shoreline run up. The justification of this is given by *Allen et al.* [1996].

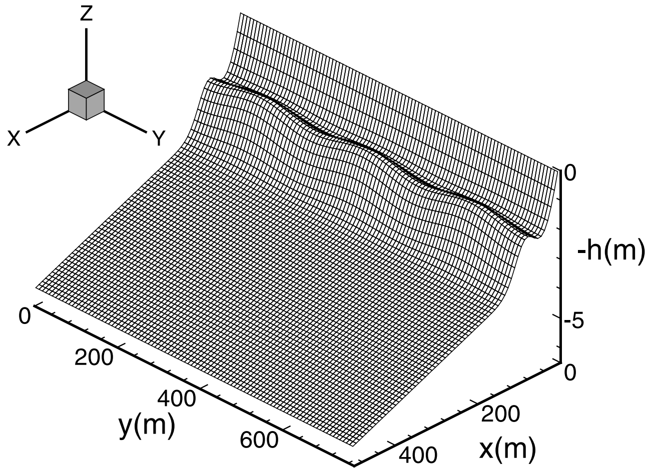

Figure 1. Beach topography with a longshore bar at $x = 80$ m and rip channels. $\epsilon = 0.1$ and $\lambda = 256$ m.

[11] The governing equations are then written as

$$(hu)_x + (hv)_y = 0, \tag{1}$$

$$u_t + uu_x + vu_y = -\frac{p_x}{\rho} + \tau_1 - \mu\frac{u}{h}, \tag{2}$$

$$v_t + uv_x + vv_y = -\frac{p_x}{\rho} + \tau_2 - \mu\frac{v}{h}, \tag{3}$$

where (u, v) are, respectively, the across-shore and longshore velocities averaged over the water depth and over the wave period, p the pressure, ρ the constant water density, μ the dimensional bottom friction coefficient, and $h = h(x, y)$ the local water depth. The shoreline is at $x = 0$. τ_1 and τ_2 are, respectively, the x and y components of the wave forcing. The bottom friction coefficient μ is related to the amplitude of the wave orbital velocity u_{wm}, which in general varies across-shore on a sloping beach. In this study, we shall use a constant μ which represents the across-shore average [*Dodd*, 1994; *Allen et al.*, 1996; *Slinn et al.*, 1998, 2000], i.e., $\mu = \frac{2}{\pi} c_f (u_{wm})_{av}$. The dimensionless friction coefficient c_f is typically of $O(0.01)$.

[12] It is worth emphasizing that the rigid lid approximation does not neglect the effect of wave set-up (set-down) on the momentum balance of currents. One of the bases of

shallow water theory is hydrostatic balance vertically, which implies that pressure is given by $p = \rho g(\eta - z)$ where η is the change of the mean water surface (set-up or set-down) relative to the undisturbed free surface at $z = 0$ and g the gravity. Thus, horizontal pressure gradients may be related to the variations of η. As is seen in equations (1)–(3), the rigid lid approximation neglects the effect of η on the continuity equation, but retains the pressure gradients in the momentum equations. The pressure p determines the set-up (set-down) through the hydrostatic equation.

[13] We note also that the velocities u and v in the shallow water equations, with or without the rigid lid approximation, are the mass transport velocities and include the mass drift due to waves. In other words, hu, for instance, represents the total transport of water across a vertical plane (y, z) per unit length, averaged over the wave period. This point is clearly made in the general treatment given by *Whitham* [1974, pp. 557–560] and *Mei* [1989, pp. 453–464].

[14] Let $\zeta = v_x - u_y$ be the vorticity in the vertical direction and $q = \zeta/h$ be the potential vorticity. We then write from equations (1)–(3) the equation for q:

$$q_t + uq_x + vq_y = \frac{1}{h}\left[\tau_{2,x} - \tau_{1,y}\right] - \frac{\mu}{h}\left[\left(\frac{v}{h}\right)_x - \left(\frac{u}{h}\right)_y\right] \tag{4}$$

Clearly, the driving force of the vorticity field is the curl of the wave forcing vector $\boldsymbol{\tau} = (\tau_1, \tau_2)$. In the absence of wave forcing and bottom friction, the potential vorticity is conserved following the flow. From equation (1) a transport stream function may be defined such that

$$hu = -\psi_y, \quad hv = \psi_x. \tag{5}$$

2.1. Wave Forcing and Wave-Current Interaction

[15] To solve the equations (1)–(3), we need a closure for the wave forcing. For small amplitude waves in irrotational flows, *Longuet-Higgins and Stewart* [1960, 1961, 1962, 1964] showed that the wave forcing effect is related to the convergence of the wave radiation stress tensor S_{ij},

$$\tau_1 = -\frac{1}{\rho h}\left(S_{11,x} + S_{12,y}\right), \qquad \tau_2 = -\frac{1}{\rho h}\left(S_{12,x} + S_{22,y}\right) \tag{6}$$

where for linear waves

$$S_{ij} = \frac{E}{2}\left\{\frac{2C_g}{c}\frac{k_i k_j}{k^2} + \left(\frac{2C_g}{c} - 1\right)\delta_{ij}\right\}. \tag{7}$$

E is the wave energy, k_1, k_2 are the wave number components in the x and y directions, respectively, and $k = \sqrt{k_1^2 + k_2^2}$. The group velocity C_g and wave phase speed c are calculated from the linear wave theory,

$$C_g = \frac{c}{2}\left(1 + \frac{2kh}{\sinh 2kh}\right), \quad c = \mathcal{F}\sigma k, \tag{8}$$

where σ is the intrinsic angular frequency of waves. Inside the surf zone, waves are no longer small amplitude nor is the flow irrotational because of wave breaking. Nevertheless, equations (6)–(7) are used to estimate the wave forcing effect across the surf zone up to the shoreline, following the hypothesis made by *Bowen* [1969a], *Longuet-Higgins* [1970], and *Thornton* [1970]. To compute the wave radiation stress, we need to know the wave field across the surf zone.

[16] When the relevant time and space scales of the topography and currents are long compared to the period and wavelength of incident waves, the wave field, in terms of local wave number, frequency and energy (wave amplitude), can be described by using the ray theory. (The phenomena associated with terms "refraction," "Doppler shift," "shoaling," "focusing," etc., are all essentially hinged to the ray theory and described by the wave equations (9), (10), (11), and (13) or (16) discussed below. In this study, we shall not distinguish those terms used in practice, but rather use "wave refraction" to refer the relevant physical processes, as by *Whitham* [1974] and by *Mei* [1989].) The equations for the wave numbers are given by [*Mei*, 1989]

$$k_{1,t} + \omega_x = 0, \tag{9}$$

$$k_{2,t} + \omega_y = 0, \tag{10}$$

where the absolute frequency ω and intrinsic frequency σ satisfy the dispersion relationship,

$$\omega = k_1 u + k_2 v + \sigma, \quad \sigma^2 = gk\tanh kh. \tag{11}$$

The two equations describe basically the conservation of wave crests, and are nonlinearly coupled due to the dispersion relationship (11). For unsteady currents, ω and σ can vary both in space and in time. It is readily deduced from equations (9) and (10) that

$$\nabla \times \boldsymbol{k} = 0. \tag{12}$$

This reflects the fact that the wave number vector $\boldsymbol{k}$ is defined as the gradient of the wave phase.

[17] In the absence of wave breaking, *Longuet-Higgins and Stewart* [1961] derived the wave energy equation, taking account of the effects of currents. For random and breaking waves, we modify the equation to include the wave energy dissipation due to breaking [*Thornton and Guza*, 1983],

$$\begin{aligned} &E_t + \left[\left(u + C_{g1}\right)E\right]_x + \left[\left(v + C_{g2}\right)E\right]_y \\ &\quad + S_{11}u_x + \tfrac{1}{2}S_{12}\left(u_y + v_x\right) + S_{22}v_y = -\epsilon_b, \end{aligned} \tag{13}$$

where ϵ_b is the ensemble-averaged energy dissipation function and

$$E = \frac{1}{8}\rho g H_{rms}^2 \tag{14}$$

the ensemble-averaged wave energy. H_{rms} is the root mean square wave height of random waves. The physical idea is that wave breaking can be modeled as a simple periodic bore and the dissipation function ϵ_b can then be constructed by following the theory of hydraulic jump [*Thornton and Guza*, 1983]. *Church and Thornton* [1993] applied

$$\begin{aligned} \epsilon_b &= \frac{3\sqrt{\pi}}{16}\rho g f_p B^3 \frac{H_{rms}^3}{h}\left\{1 + \tanh\left[8\left(\frac{H_{rms}}{\gamma h} - 1\right)\right]\right\} \\ &\quad \cdot \left\{1 - \left[1 + \left(\frac{H_{rms}}{\gamma h}\right)^2\right]^{-2.5}\right\} \end{aligned} \tag{15}$$

to the beach in DELILAH field experiments at Duck, North Carolina. They found that the predicted wave height distribution across-shore agreed reasonably well with observations. Across the front of a bore, the energy loss is determined by the properties of the flow relative to the front [*Stoker*, 1957]. In the presence of unsteady currents, the wave frequency varies and f_p in equation (15) should be related to the intrinsic frequency, i.e., $f_p = 2\pi/\sigma$. There are two empirical coefficients in ϵ_b. B represents the fraction of foam on the face of waves and loosely accounts for different types of breakers. γ indicates the saturation of breaking. In other words, all waves should break when their wave heights reach to γh. In our numerical experiments, $B = 1.3$ and $\gamma = 0.38$. These are in the range of the values used to fit the data in DELILAH experiments [*Church and Thornton*, 1993; *Lippmann et al.*, 1996].

[18] The last three terms on the left-hand side of equation (13) have an important physical meaning. They represent the transfer of energy to (or from) waves due to the work done by radiation stresses acting on the strain of currents. For instance, a negative value of the sum of these three means that waves gain energy at the expense of currents. Unlike the flux terms $\partial/\partial x_j[(u_j + C_{gj}) E]$ in equation (13), which only carry in wave energy at the offshore boundary and redistribute the energy inside the domain, these radiation stress terms act like energy sinks or sources inside the domain. We shall see in section 3.1 that the strain of rip currents indeed plays a significant role in changing the wave energy, and subsequently the wave forcing on the currents. Using equations (9) and (10), an equation for wave action, E/σ, can be derived from equation (13) [*Mei*, 1989, pp. 96–98],

$$\left(\frac{E}{\sigma}\right)_t + \left[\left(u + C_{g1}\right)\frac{E}{\sigma}\right]_x + \left[\left(v + C_{g2}\right)\frac{E}{\sigma}\right]_y = -\frac{\epsilon_b}{\sigma} \tag{16}$$

This says that in the absence of wave dissipation the wave action is conserved following wave rays. Note that the radiation stress terms which appear in the energy equation (13) are now absorbed into σ. When the process is interpreted in terms of wave action, it is then clear that the change of wave energy due to work done by radiation stress is also an effect of refraction by currents.

[19] When currents are weak compared to the wave group velocity, their effects on waves are small, but such effects are sometimes not negligible. This is the case for rip currents produced by alongshore topographic variations on otherwise alongshore uniform beaches. Without such variations, it is readily seen that $\tau_1 = \tau_{10}(x)$ and $\tau_2 = 0$ for normally incident waves. The curl of the wave forcing is zero, and vorticity cannot be generated from rest according to equation (4). Hence no flow is produced based on this two dimensional shallow water theory, except at transient state, and the nonzero wave forcing $\tau_{10}(x)$ is entirely balanced by the across-shore pressure gradient (wave set-up/set-down). However, alongshore variations in the topography, like gentle rip channels, produce longshore variations in the radiation stress giving that

$$\tau_1 = \tau_{10}(x) + \tilde{\tau}_1(x,y), \quad \tau_2 = 0 + \tilde{\tau}_2(x,y) \tag{17}$$

where $\tilde{\tau}_1$ and $\tilde{\tau}_2$ are of $O(\epsilon)$, the magnitude of the longshore topographic variations. The curl of $(\tilde{\tau}_1, \tilde{\tau}_2)$ is generally not zero, and this provides the source of vorticity and of horizontal circulations with which we are here concerned. The circulations interact with waves, and the wave radiation stress will be subsequently modified. Such changes of course are small relative to the effects due to wave breaking, but can be comparable to the variations caused by the topography. When this is the case, the circulations of interest can be significantly affected by the wave-current interaction.

[20] On the contrary, the source of the alongshore current momentum comes from $S_{12,x}$ of the obliquely incident waves, and the source of vorticity is $S_{12,xx}$. Wave breaking across the surf zone is the primary cause of such x variations. Effects of wave-current interaction may modify the radiation stress, but such changes must be small compared to those due to breaking, unless the currents are sufficiently strong. In fact, as waves gradually turn normally to the shoreline, they will be even less affected by the mean currents alongshore. It then seems to be quite justifiable to neglect the effects of the alongshore currents on waves. When such alongshore currents become unstable (shear instabilities), the subsequent evolution of the instabilities may, however, still be considerably different depending on whether or not the interaction is included.

2.2. Boundary Conditions

[21] The domain of computations is $0 \leq x \leq L^x$ and $0 \leq y \leq L^y$. For the shallow water equations describing currents, it is necessary to require vanishing across-shore mass flux at the shoreline and at the offshore boundary, i.e.,

$$hu = 0 \quad \text{at} \quad x = 0 \quad \text{and} \quad L^x. \tag{18}$$

In the alongshore direction, periodic conditions are imposed on u, v and p because of the topography and the nature of the flow we are interested in. To eliminate small scale disturbances arising from the finite difference approximations to the differential equations, biharmonic dissipation, $-\nu\nabla^4 u$ and $-\nu\nabla^4 v$, are added to the right-hand side of the momentum equations (2) and (3), respectively [*Allen et al.*, 1996; *Slinn et al.*, 1998, 2000]. Corresponding to these, the following additional boundary conditions are required,

$$u_{xx} = v_x = v_{xxx} = 0 \quad \text{at} \quad x = 0 \quad \text{and} \quad L^x, \tag{19}$$

which may be interpreted as an analog of the free slip condition with ordinary viscosity.

[22] For incoming waves, the incidence angle θ is specified at the deep sea, and then transferred to the offshore boundary using Snell's law. The incident wave height H_0 is simply specified at the offshore boundary. Note that to produce rip currents, waves have to be normally, or near normally, incident. Otherwise, longshore currents dominate; see section 3.3.

2.3. Numerical Procedure

[23] To couple waves and currents, we time integrate the equations for currents and for waves. The numerical scheme of solving the shallow water equations (1)–(3), with the boundary conditions (18) and (19), is described in detail by *Allen et al.* [1996] and *Slinn et al.* [1998, 2000]. For numerical efficiency, the wave action equation (16) is

solved instead of the wave energy equation (13). The wave number field is obtained from equations (9) and (12) in order to preserve the irrotationality of (k_1, k_2). We apply the first-order Euler method in time, first-order upwind differencing in x and central finite differencing in y. To check the accuracy, we solved the steady state equations for waves, with no currents, using a higher-order scheme on the grid $\Delta x = \Delta y = 2$ m. Good agreement was found between this and the steady state solution obtained from the time integration on the same grid. As for Δt, the time step required for numerical stability is so small compared to the physical time scales involved in currents and waves that the accuracy seems to be controlled mainly by the spatial differencing.

[24] In all the numerical experiments, $\Delta t \leq 0.2$ s and $\Delta x = \Delta y = 2$ m. The biharmonic friction coefficient $\nu = 1.25$ m^4/*s*, which adds numerical damping at length scales smaller than 4 m and has little influence on the scales of currents and waves [*Slinn et al.*, 2000]. The currents start from rest in each experiment. The initial wave field is the steady state solution with no current. A small perturbation is added to the velocity field just at $t = 40$ min in order to trigger any instabilities. In some cases, however, instabilities develop sooner.

3. Results

[25] In the experiments presented below, the period of incoming waves is $T = 10$ s. $\Delta t = 0.1$ s in most cases. In a few cases of steady circulations, $\Delta t = 0.2$ s was used. Two lengths of the across-shore domain are used: $L^x = 500$ m and 800 m. The longer length is used to ensure that $u \simeq 0$ as $x \rightarrow L^x$ in the cases where rip currents are strong. This affects little the offshore boundary condition of the wave height, because of the small beach slope. The computations show that the wave heights at 800 m and 500 m are different by less than 5%. The length of the longshore domain is always a multiple of the spacing of rip channels.

3.1. Physical Significance of Wave-Current Interaction

[26] In this section we shall illustrate by two computations that major differences can occur when wave-current interaction is taken into account. An explanation of the physics behind these differences follows.

[27] Figure 2a shows the transport stream function and vorticity contours at $t = 80$ min from the computation with the wave-current interaction. Waves are incident normally, i.e., $\theta = 0°$, and the wave height at the offshore boundary $H_0 = 1$ m. The magnitude of the bottom perturbation $\epsilon = 0.1$ and the spacing of rip channels $\lambda = 256$ m. The bottom friction $\mu = 0.002$ m/s. For the same parameters, the results from the computation without the interaction are presented in Figure 2b, in which the wave field and wave forcing are computed only once at $t = 0$ before currents develop and held fixed thereafter. From these figures the following common features are observed.

1. In both computations, cellular circulation patterns are seen in the stream function contours. The flow is offshore directed at rip channels, cf. $y = 0$, 256, 512, and 768 m, and onshore over the transverse bar crests at $y = 128$, 384, and 640 m. Indicated by the density of contours, the offshore flow is narrower and stronger than the onshore flow even though the alongshore topographic variation is sinusoidal.

2. Rip currents are fed by the longshore flows in the region at 40 m $< x <$ 80 m. Note that the crest of the alongshore bar is located at $x = 80$ m, and trough at $x = 40$ m. In other words, the feeder flow is at the shoreward face of the alongshore bar.

3. Strong vorticity is observed in the rip currents, and in the flow close to the shoreline where the water is shallow. However, the following marked differences are also evident from the numerical simulations.

1. With no wave-current interaction, rip currents can reach offshore to about 600 meters from the shoreline even with this moderate bottom friction coefficient and wave height. With the interaction, the distance is reduced by more than half. This is consistent with *Haas et al.* [1998]. Circulations are mostly within 240 meters from the shoreline, approximately two times the distance from the shoreline to the location where intensive wave breaking starts.

2. Without the interaction, it is observed that the offshore extent of rip currents increases with decreasing bottom friction μ. This distance is, however, not significantly affected by a change of μ (see section 3.2.1) when the interaction is included.

3. Comparing the stream function contours in Figure 2a and Figure 2b, rip currents are noticeably broader and weaker when the interaction is included. In fact, the maximum offshore u velocity is reduced by about half, but the maximum onshore u velocity remains approximately the same. This suggests that the narrow offshore rip currents have stronger effects on the wave field.

4. The circulations become unstable in different manners. Without the interaction, the onset of instabilities occurs offshore such that the rip heads start wobbling. Gradually, instabilities work their way onshore, see Figure 3. With the interaction, the flow for this set of parameters is stable. However, in the cases where circulations do become physically unstable, instabilities always occur initially at the longshore trough where rips are fed, characterized by ejection of vorticity into rip channels and offshore migration of vortex pairs. We shall see details in section 3.3.

[28] So what causes the differences? Explanation must be sought from the wave forcing because that is how the waves and currents are coupled. In section 2.1 we showed that circulations are generated due to the alongshore variation of the wave forcing. Let us denote the alongshore mean by $\langle\cdot\rangle$ and the deviation from the mean by $\sim$, and decompose the wave forcing into two parts,

$$\tau_1 = \langle\tau_1\rangle + \tilde{\tau}_1(x, y), \quad \tau_2 = \langle\tau_2\rangle + \tilde{\tau}_2(x, y), \qquad (20)$$

For normally incident waves, $\langle\tau_2\rangle = 0$ and the alongshore means have no contribution to the source of vorticity which is $\nabla \times \boldsymbol{\tau}$ and $\boldsymbol{\tau} = (\tau_1, \tau_2)$. For near normally incident waves, $\langle\tau_2\rangle \neq 0$ but small. It is mainly responsible for a weak alongshore averaged alongshore flow which breaks the symmetry of the circulation cells. For clarity, we base the following discussion on the normally incident waves. It is noted that $\langle\tau_1\rangle$ is negative, and is the major part of τ_1. This reflects the shoreward decrease of wave energy in the surf zone due to breaking, i.e., a positive value of $\langle S_{11,x}\rangle$. It is merely responsible for a longshore averaged pressure gradient $\langle\partial p/\partial x\rangle$, since it does not produce vorticity.

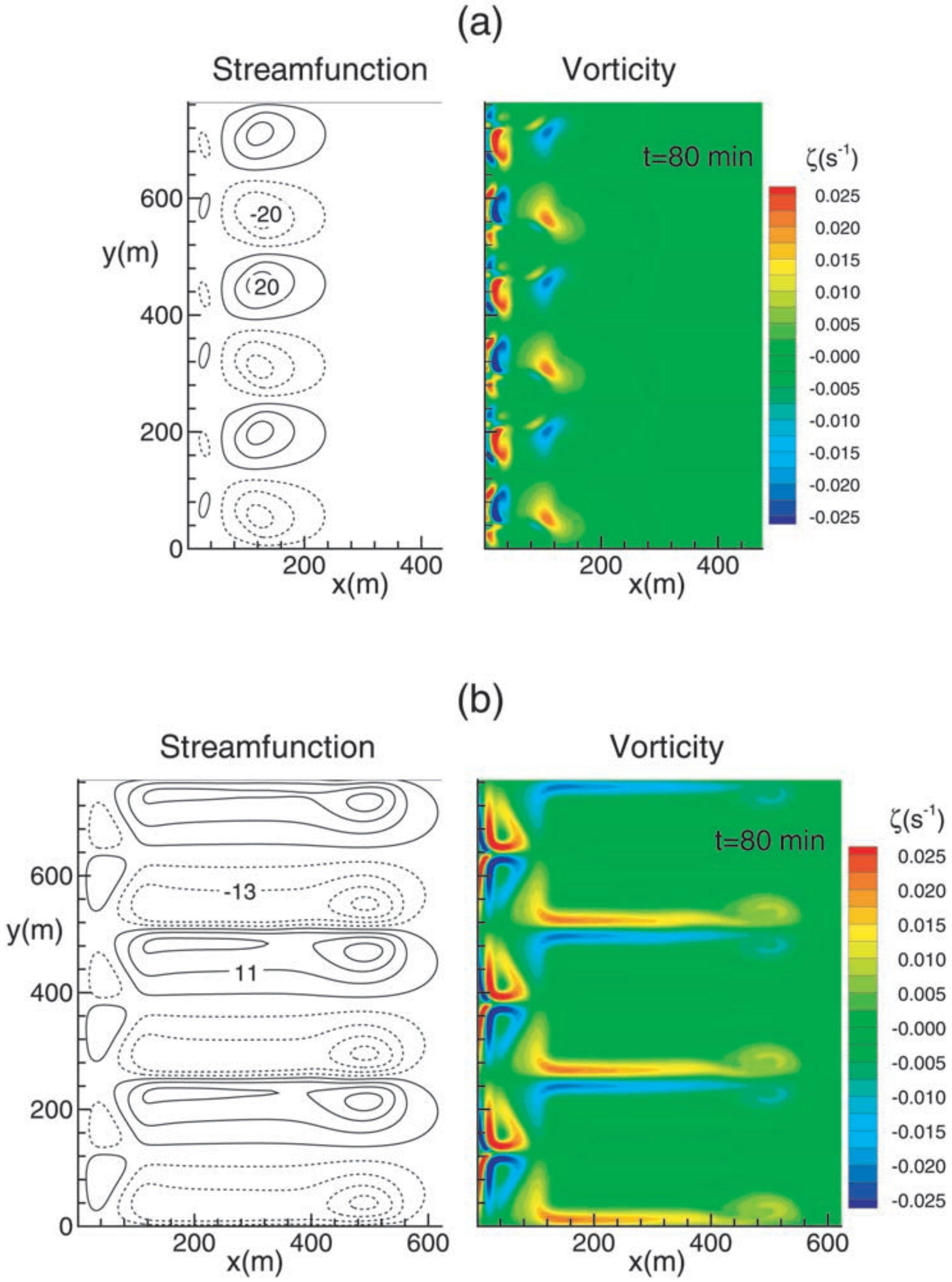

Figure 2. Contours of stream function and vorticity at t = 80 min from the computation: (a) with the wave-current interaction and (b) without the interaction. Parameters are $\theta = 0°$ and H_0 = 1 m at offshore, μ = 0.002 m/s, ϵ = 0.1, and λ = 256 m. Increment of stream function $\Delta\psi$ = 6 m^3/s.

[29] Figures 4a, 4b, and 4c show the contours of the deviations $\widetilde{\tau}_1, \widetilde{\tau}_2$, and $\nabla \times \boldsymbol{\tau}$ at t = 0, respectively. Before currents develop, these deviations arise due to the alongshore variation of the topography. Compared to $\widetilde{\tau}_1$, the y component $\widetilde{\tau}_2$ is weak and concentrated at the shoreline. Thus, $\nabla \times \tau \simeq -\widetilde{\tau}_{1,y}$ away from the shoreline. From Figure 4a, $\widetilde{\tau}_1$ is negative over the transverse bar crests at x = 100 m and y = 128, 384, and 640 m, and positive at rip channels at y = 0, 256, 512, and 768m, thus provides the initial sources of onshore flows and offshore rip currents, respectively. Over a transverse bar crest, the wave height tends to increase due to refraction by the topography, and the water depth is reduced. Both of these enhance the breaking and the transfer of wave momentum into currents. Therefore, the deviation $\widetilde{\tau}_1$ should be negative, the same as the alongshore mean, so as to produce stronger forcing τ_1 (than the mean). The reverse is true at rip channels. Correspondingly, the sources of vorticity are then found to be positive on the north side (assuming the shoreline is on the west) of a rip channel and negative on the south side; see Figure 4c at x = 100 m. Note that the sources of vorticity are symmetrically distributed at the channels and transverse crests. Once circulations

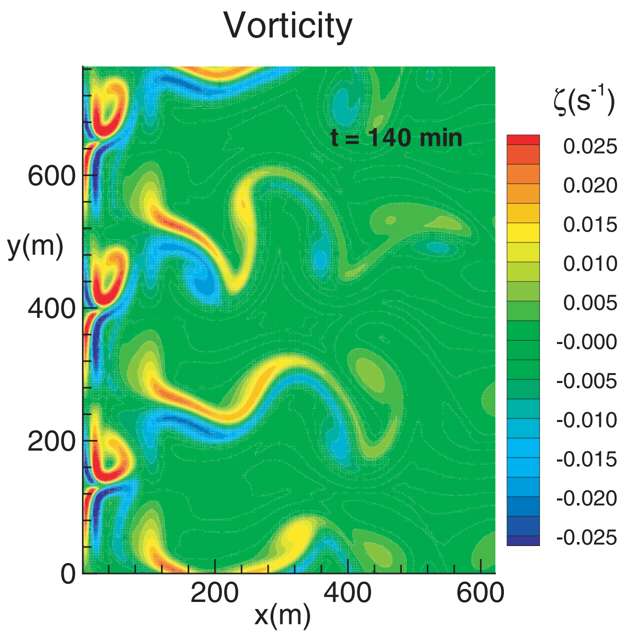

Figure 3. Contours of vorticity at t = 140 min from the computation in Figure 2b.

are generated, the longshore flows at the longshore trough converge toward a rip channel and diverge away from a transverse bar crest. Thus, vorticity tends to be advected into a rip channel and away from a transverse bar crest. This leads to the concentrated vorticity patches in the rip channels and near absence of vorticity over the crests; see Figure 2b. As a result, the rip currents are narrow and strong, and the onshore flows are broad and weak. This is consistent with *Arthur* [1962] and *Bowen* [1969b] that nonlinearity is important to produce narrow offshore directed rip currents. If the effect of currents on waves is neglected, such a forcing pattern persists. Vorticity will constantly be generated by the sources and advected offshore by rip currents. In the offshore region, there is practically no wave forcing and little bottom friction because of the great water depth. Therefore, vorticity can migrate to a great distance, leading to long streams of vorticity offshore at rip channels; see Figure 2b.

[30] The wave field, however, is changed due to the interaction with the developing currents. Figures 4a′, 4b′ and 4c′ plot the contours of $\tilde{\tau}_1, \tilde{\tau}_2$, and $\nabla \times \boldsymbol{\tau}$ at $t = 40$ min, respectively. Now the positive x forcing $\tilde{\tau}_1$ at rip channels is reduced in strength, and cut into three pieces by a ring of negative forcing, see Figure 4a′. The offshore directed rip currents evidently interact with the incoming waves and produce a forcing effect opposite to that due to the topography. While reduced forcing produces weaker rip currents, the slightly negative forcing at offshore exits of rip channels (x = 130 m) decelerates rip currents such that vorticity cannot be advected so far offshore. Circulations are then confined to the nearshore. Comparing Figure 4b and Figure 4b′, the y forcing $\tilde{\tau}_2$ at the alongshore bar (x = 80 m) becomes stronger after currents develop, and extends further offshore. This tends to accelerate the alongshore flows, diverging away from the rip currents, thus broadening the rip currents and reducing their strength. It is also noted that the y forcing at the shoreline is broken into smaller pieces and stretched into the alongshore trough at x = 40 m. In Figure 4c′, the positive vorticity source on the north side of a rip channel seen at $t = 0$ is now broken into a triplet with a strong negative source in the middle. A similar result occurs for the negative source on the south side. Close to the shoreline, the sources of vorticity become more complex and exhibit smaller scales.

[31] The effects in the forcing seem to occur due to two physical processes involved in the interaction: (1) changes in wave rays (i.e., wave numbers) and (2) changes in wave energy (or amplitude). For normally incident waves over the topography of interest, $|k_2| \ll |k_1|$, and $C_g \simeq c$ in shallow water. From equation (7) we have approximately

$$S_{11} \simeq \frac{3}{2}E, \quad S_{12} \simeq -\frac{k_2}{|k_1|}E, \quad S_{22} \simeq \frac{1}{2}E. \tag{21}$$

Let us focus on the x forcing which comes from $-S_{11,x}$ and $-S_{12,y}$, see equation (6). Though S_{12} is small compared to S_{11}, the longshore variable part of S_{12}, which is all of it, is comparable to that of S_{11}. So they both are important to the longshore variation of the x forcing. It is readily seen that $S_{12,y} \simeq -Ek_{2,y}/|k_1|$ because the fractional changes in k_2 due to bending of wave rays are large compared to those in E and k_1. Before currents develop, the topographic refraction causes wave rays to bend away from the center of a rip channel, i.e., $k_{2,y} > 0$ across the channel. The offshore directed rip currents, however, tend to bend wave rays toward the center of the currents, hence reduce $k_{2,y}$ or even make it negative. As a result, $S_{12,y}$ decreases in magnitude, and in fact even reverses its sign when currents get strong enough. On the other hand, offshore at a rip channel ($x > 80$ m) u, v and C_{g2} are all small compared with C_{g1}, and in this region the wave energy equation (13) can be approximated as:

$$\frac{\partial E}{\partial t} + \frac{\partial}{\partial x}\left(C_{g1}E\right) + S_{11}\frac{\partial u}{\partial x} + S_{22}\frac{\partial v}{\partial y} = -\epsilon_b \tag{22}$$

Offshore the flow is decelerating because it is broadening, so $\partial u/\partial x < 0$. From the continuity equation (1), we have $u_x + v_y \simeq -uh_x/h < 0$. Since S_{11} is approximately three times of S_{22}, the sum of the two radiation stress terms in equation (22) is negative. Work is then done on waves by radiation stresses to increase the wave energy offshore at a rip channel. The reverse is true at a transverse bar crest. These can be seen clearly in Figure 5, see $x > 100$ m at $t = 0$, and at t = 40 min. Compared with those in the neighboring region, waves propagating toward rip currents will break sooner, which is commonly observed, and more strongly because of the greater wave height. Again, rip currents produce an effect opposite to that due to rip channels (which reduce breaking). They thereby reduce the magnitude of $S_{11,x}$ produced by topography, in particular near the intensive breaking zone. Since the topographic effect exists only when rip channels are present, the effect due to currents becomes more dominant as rip currents flow offshore and reverses the sign of the alongshore variable x forcing, i.e., $\tilde{\tau}_1$ becomes negative, see Figure 4a′ at x = 130 m.

[32] Without interaction, the flow at rip heads far offshore is practically frictionless because of the great depth; while

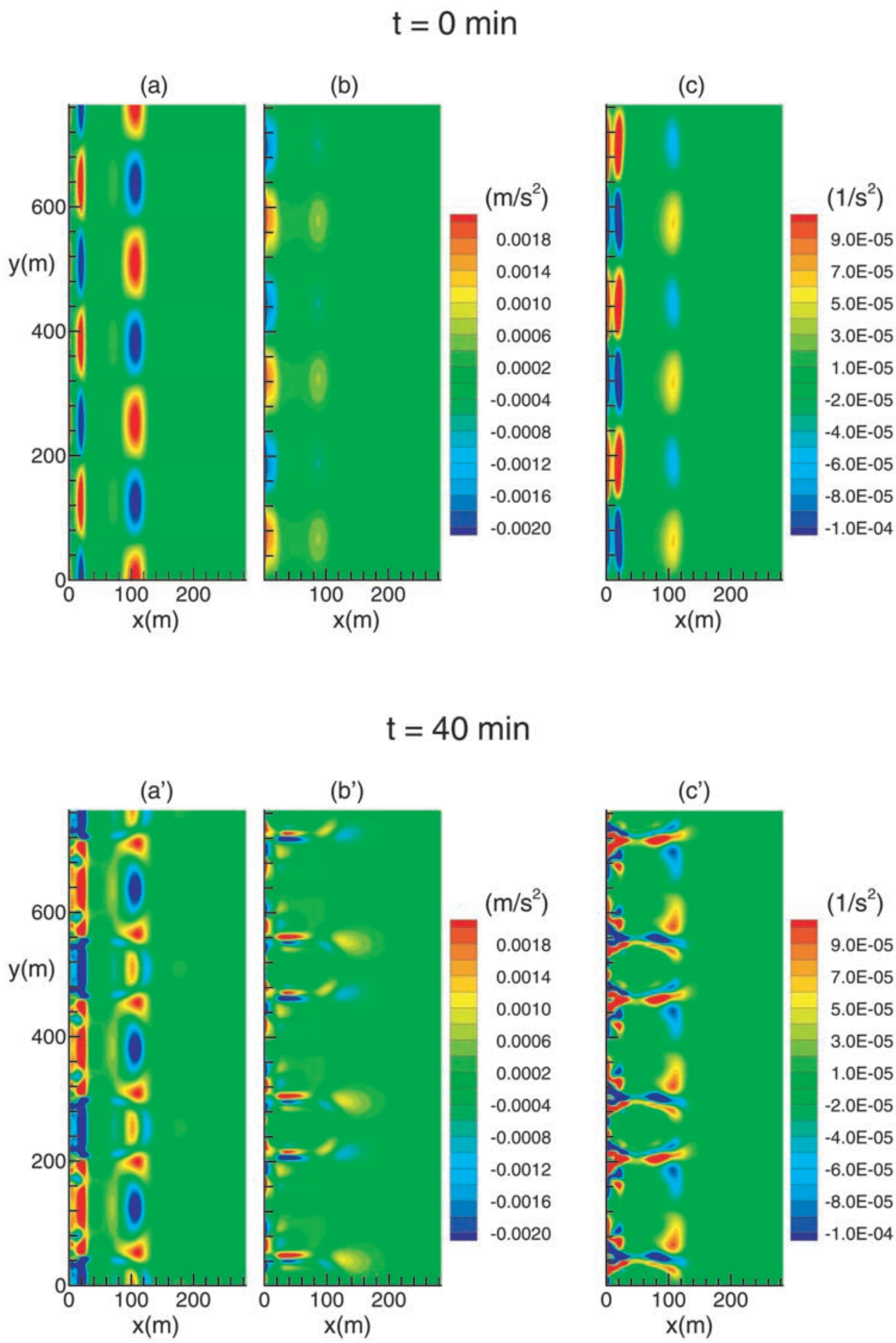

Figure 4. Deviations of the wave forcing from its longshore mean before (t = 0) and after (t = 40 min) currents develop: (a) the x component, $\tilde{\tau}_1$, (b) the y component, $\tilde{\tau}_2$, and (c) the curl of the wave forcing $\nabla \times \boldsymbol{\tau}$. Parameters are the same as in Figure 2.

close to the shoreline, the flow may have stronger shear but the bottom friction is also much stronger. Therefore, instabilities may develop relatively easier offshore. Second, similar to a jet flow in a finite domain, it takes space for instabilities to develop. Thus, the instabilities at rip heads may be just the first to be seen. With the interaction, however, the flow is mostly in the region close to the shoreline, hence frictional everywhere. On the other hand, at the entrance of rip channels, the across-shore flow is accelerating (u_x > 0), because of the convergence of the alongshore flows. From the wave energy equation, $S_{11}u_x > 0$. Thus the work done by radiation stress can cause waves to

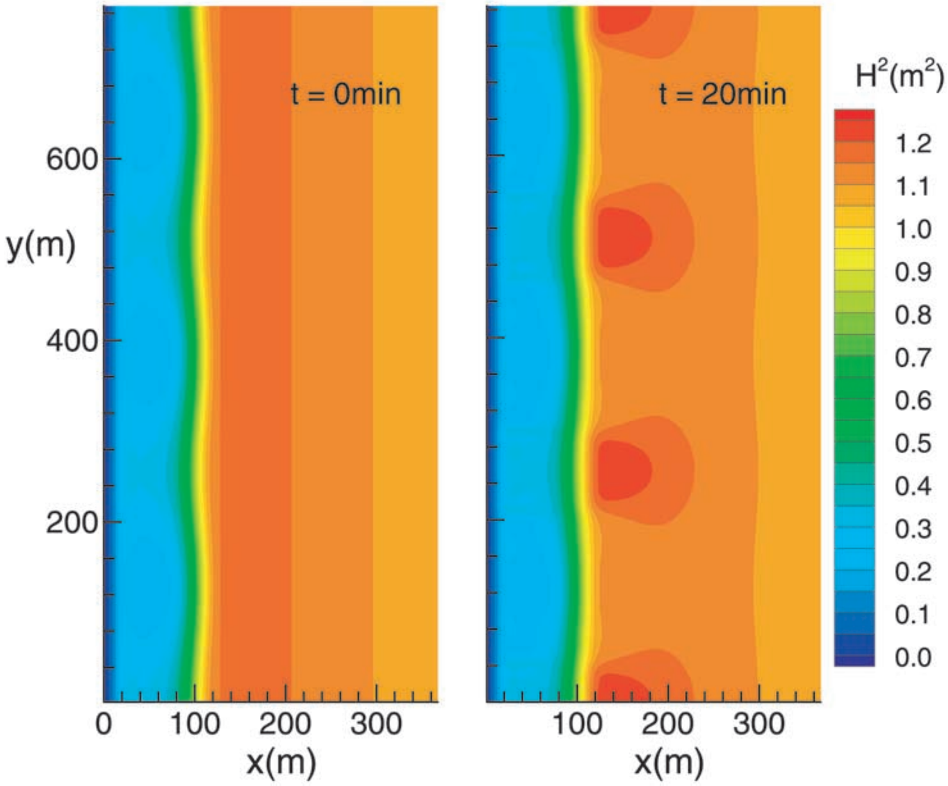

Figure 5. Contours of the square of the wave height at $t = 0$ and $t = 40$ min. Parameters are the same as in Figure 2.

lose energy to currents, perhaps resulting in more energetic currents at the entrance of rip channels, which might contribute to the instability at the feeder region. A more definitive explanation requires a systematic study of instabilities of the circulations coupled to waves. Relatively little is known about instabilities of any kind of nonparallel flow.

3.2. Basic Features of Rip Currents

[33] In this section we will discuss some of the main features of rip currents, such as their strength, offshore extent and width (longshore extent). Cases presented are mostly those which evolve into steady cellular circulations, though a few unsteady ones are included. For such cases, time averaged flows, over 8 hours from $t = 120$ min to $t = 600$ min, are used to define rip features. To facilitate quantitative comparison, we define the offshore extent of rips as the maximum offshore reach of the contour $u = 0.01$ m/s, and the width of rip currents as the longshore extent of the same contour at $x = 160$ m, two times the offshore distance of the longshore bar. For each parameter to be discussed below, μ, H_0, ϵ and λ, we plot the across-shore profiles of the u velocity along the center line of a rip channel ($v \simeq 0$ along this line), and the variations of the offshore extent and width of rips with that parameter; see Figures 6, 7, 9, and 10.

3.2.1. Effects of Bottom Friction

[34] In this set of experiments, the rip channel spacing $\lambda = 256$ m and $\epsilon = 0.1$. The domain of the computations is $L^x = 500$ m and $L^y = 768$ m. Waves are normally incident and their height at the offshore boundary H_0 is 1 m. In Figure 6a, seaward of the longshore bar ($x > 80$ m), the u velocity profiles are approximately the same for all the bottom frictions and have maxima located at $x = 130$ m, slightly seaward of the line where intensive breaking first occurs, see Figure 5 at $x \simeq 100$ m. As μ decreases, another maximum emerges at $x = 17$ m. In all the profiles, a nonzero minimum occurs at $x = 40$ m, near the longshore trough where rips are fed. In Figure 6b the offshore extent and width of the rip currents are both weakly dependent on the bottom friction. In the experiments with no wave-current interaction (not shown), the offshore extent increases with decreasing μ. This is anticipated because the bottom friction is the only dissipative effect on the flow if the wave-current interaction is not included. With the interaction, however, the effects of currents result in a negative wave forcing at the offshore exits of rip channels (see section 3.1), which decelerates the currents as they flow seaward. This self-produced dissipation is dominant because the bottom friction is so small when the water depth is large.

[35] In addition to demonstrating the significance of the wave-current interaction, the results in Figure 6 suggest definitely that bottom friction becomes less influential to the prediction of flow patterns. In view of the uncertainty in the bottom friction parameterization, this finding is particularly valuable.

3.2.2. Effects of Incoming Wave Conditions

[36] Two important physical parameters of the incoming wave conditions are the wave height H_0 and the incidence angle θ. To test the effects of the wave height, we utilize the

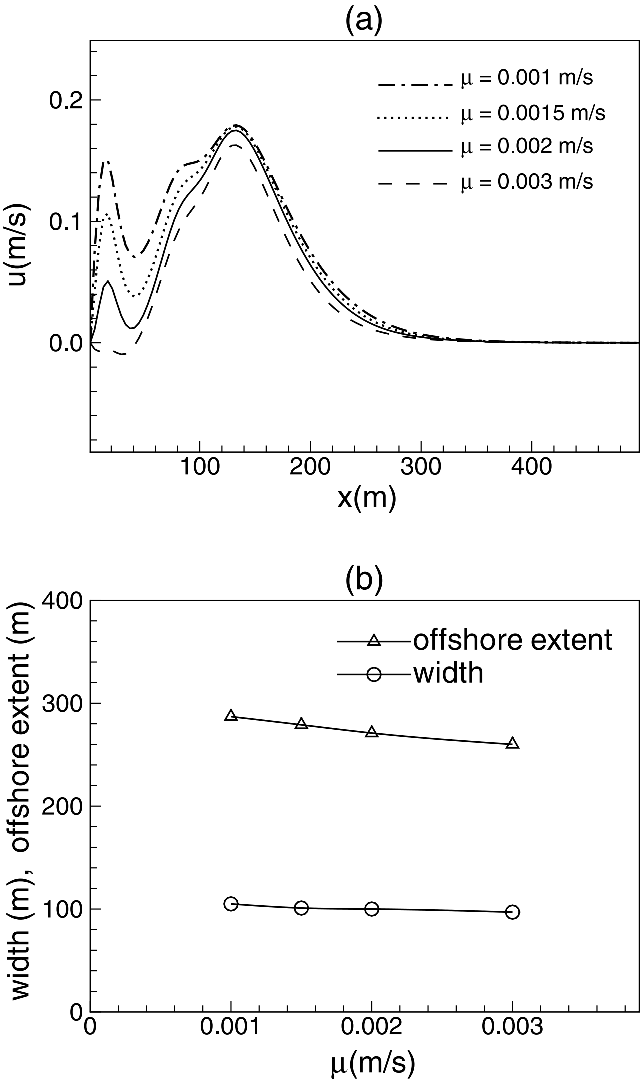

Figure 6. (a) Across-shore profiles of the *u* velocity at y = 256 m, the centerline of a rip channel. (b) Variations of the offshore extent and width of rip currents with bottom friction μ. θ = 0° and H_0 = 1 m at offshore. ϵ = 0.1 and λ = 256 m.

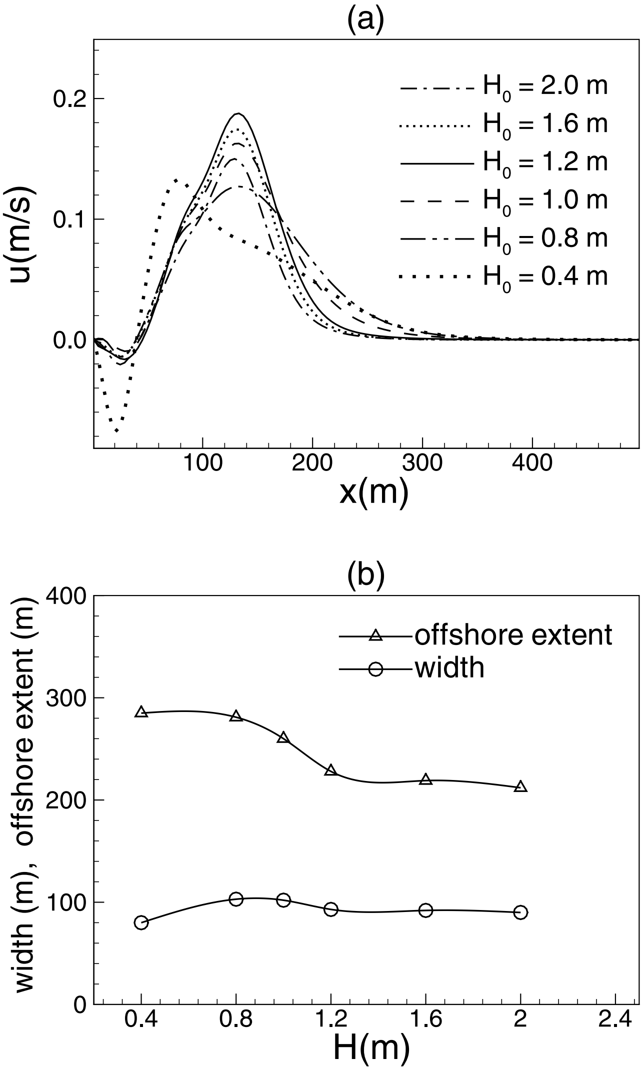

Figure 7. (a) Across-shore profiles of the *u* velocity at y = 256 m, the centerline of the rip channel. (b) Variations of the offshore extent and width of rip currents with the height of incoming waves. θ = 0°. ϵ = 0.1 and λ = 256 m. For μ, see text.

same topography as in section 3.2.1, again with normally incident waves, comparing H_0 = 0.4, 0.8, 1.0, 1.2, 1.6 and 2.0 m. Correspondingly, we use the bottom friction $\mu \simeq$ 0.0013, 0.0025, 0.003, 0.0038, 0.005 and 0.0064 m/s, which have been chosen so that the dimensionless bottom friction coefficient $c_f \simeq 0.0094$ in all cases because of the dependency of μ on the wave height, cf. section 2. For H_0 = 0.8 m and μ = 0.0025 m/s, the flow is weakly unstable, oscillating periodically with small amplitude; see section 3.3. In all other cases steady flows develop.

[37] For $H_0 \geq 0.8$ m in Figure 7a the maximum rip current velocity is located approximately at x = 130 m. For H_0 = 0.4 m, it is located at x = 78 m. The value of the maximum velocity increases as H_0 varies from 0.8 m to 1.2 m, and then decreases as H_0 is further increased to 2.0 m. Figure 8 shows the wave height variations along y = 256 m and y = 384 m (dashed). It indicates that (i) H_0 = 0.4 m is too small for the wave to break even on the longshore bar, breaking only in very shallow water at x = 20 m; (ii) all the other cases have intensive breaking at the seaward face of the alongshore bar, around x = 120 m, and very similar wave height distributions further toward the shore (with strong breaking again in even shallower water, much like the case H_0 = 0.4 m); (iii) the two largest cases exhibit

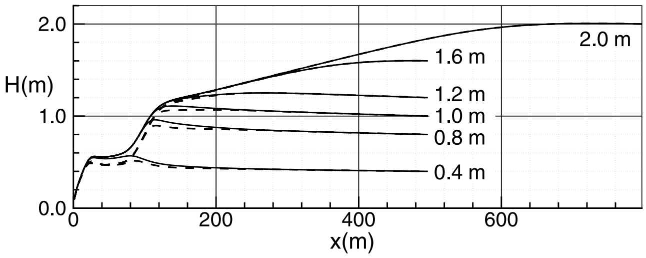

Figure 8. Wave heights across shore at y = 256 m and at y = 384 m (dashed) for the experiments in Figure 7.

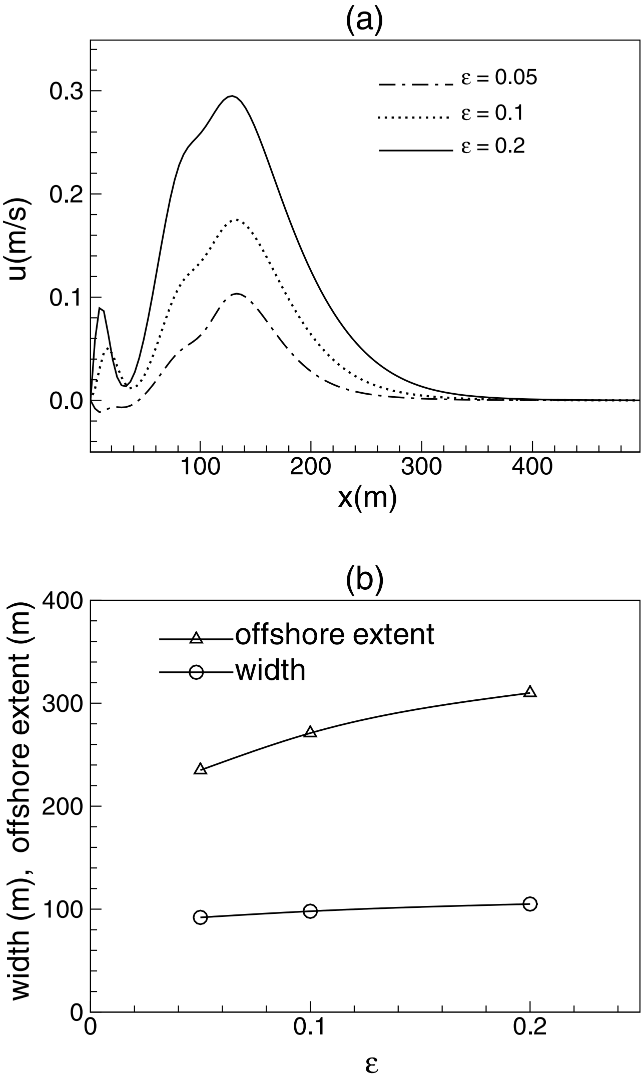

Figure 9. (a) Across-shore profiles of the u velocity at y = 256 m, the centerline of the rip channel. (b) Variations of the offshore extent and width of rip currents with ϵ. $\theta = 0°$ and H_0 = 1 m. μ = 0.002 m/s and λ = 256 m.

appreciable breaking well offshore of the longshore bar, and beyond the extent of rip channels and rip currents; and (iv) the wave heights are slightly smaller over the bar crest compared to that at the rip channel.

[38] For $H_0 \leq 1.2$ m, the position of the maximum rip current velocity (at $x \simeq 130$ m) is a little offshore of the breaking line (at $x \simeq 120$ m). For $H_0 \geq 1.6$ m, since there are no rip channels (or longshore variation in the topography) where the waves first start to break (at $x > 400$ m), rip currents are not developed in this region. The smallest wave H_0 = 0.4 m also has no rip channels where it starts to break close to the shore, but the waves have been refracted when passing over the barred region so longshore variation is present in the breaking region. The decrease of offshore extent of rip currents with H_0 is evident in Figure 7b, and it is also confirmed in Figure 7a. The width of rips shows a little variation with wave height H_0.

[39] For obliquely incident waves, the simulations show that for this beach topography with ϵ = 0.1 the flow develops into longshore currents, characterized by meandering longshore streamlines rather than closed cells, when the incidence angle at the deep sea (measured clockwise from the x axis) is greater than 5°. Using Snell's law, for 10 second waves, this means that the incidence angle at the offshore boundary, say L^x = 500 m, has to be smaller than 2.3° for cellular circulations to occur. The circulations at small angles, however, are mostly turbulent, associated with vortex shedding and pairing. This is not inconsistent with the observation that in nature rip currents are often found to be unstable and transient, since waves are rarely perfectly normal. We shall discuss the development of turbulent rip currents in section 3.3.

3.2.3. Effects of Topography

[40] We have examined the effects of rip channel depth and spacing. In the first set of experiments, we fix the spacing of rip channels to be λ = 256 m and vary the depth of rip channels by setting ϵ = 0.05, 0.1, 0.2. Waves are normally incident with H_0 = 1 m at the offshore boundary and μ = 0.002 m/s. We note that the magnitude of the alongshore variation is stronger as ϵ increases, but the length scale of the variation remains the same because λ is fixed. From Figure 9a the maximum velocity of the rip currents increases almost linearly with ϵ, while the position of the peak velocity remains at x = 130 m. In other words, the velocity profile does not change its across-shore shape as ϵ varies. The offshore extent of rips increases with ϵ somewhat less than linearly, see Figure 9b, but the width is not significantly affected by varying ϵ.

[41] In the second set of experiments, we keep ϵ = 0.1 and vary the rip channel spacing λ = 1024/6, 1024/4, 1024/3, 840/2 and 1024/2 m. L^y = 1024 m or 840 m. L^x = 500 m for the two smallest λ and L^x = 800 m for the rest. H_0 = 1 m at $x = L^x$ and $\theta = 1°$ at the deep sea. The bottom friction μ = 0.003 m/s. In the case of the largest spacing λ = 512 m, the flow is turbulent. The position of the maximum rip current velocity moves seaward noticeably as λ increases; see Figure 10a. This is found to be true too for the locations of maximum hu, though to a less extent. None of the previously examined parameters, μ, H_0 and ϵ, have such a strong effect on this position. It is also noticed that the maximum velocity decreases with λ. This is consistent with the result of varying ϵ, since increasing λ or decreasing ϵ each produces weaker alongshore variation. However, varying λ for a fixed ϵ changes the length scale of the alongshore variation in addition. This perhaps is responsible for the broadening and offshore shift in the velocity profiles as λ increases; see Figure 10a. Consistently, the offshore extent of the rip currents shows a marked increase with λ; see Figure 10b.

[42] Since the bottom perturbation is sinusoidal, the spacing of rip channels measures also the width of the channels. From Figure 10b the width of rips is nearly linear with λ. In the other experiments just discussed, where λ is fixed, the width of rips shows little variation with the physical parameters examined. This suggests that the width of the well developed rip currents is determined by the width of the channels.

3.3. Unsteady Circulations

3.3.1. Main Properties

[43] Figure 11 shows time series of the across-shore and longshore velocities at x = 101 m and given y locations for a

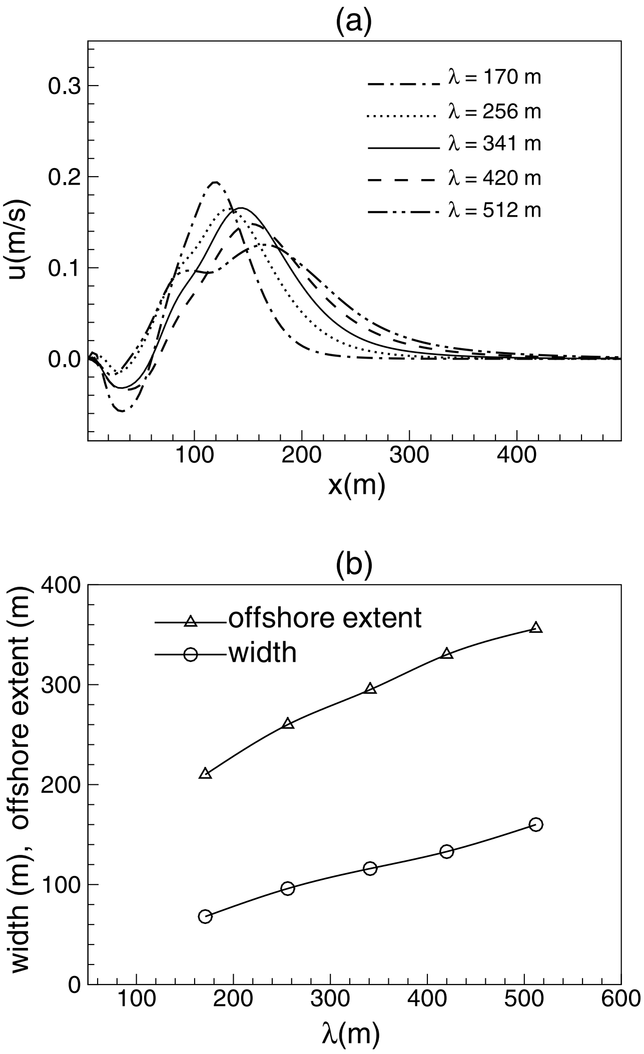

Figure 10. (a) Across-shore profiles of the u velocity at the centerline of a rip channel. (b) Variations of the offshore extent and width of rip currents with λ. $\theta = 1°$ and $H_0 = 1$ m. $\epsilon = 0.1$ and $\mu = 0.003$ m/s.

set of experiments with small incidence angles. Wave height $H_0 = 1$ m at the offshore and the incidence angles $\theta = 1°$, $3°$, $5°$ and $10°$ at the deep sea. $\mu = 0.003$ m/s. $L^x = 500$ m and $L^y = 768$ m. Rip channels are located at $y = 0$, 384, and 768 m and $\epsilon = 0.1$. Correspondingly, the time averaged (denoted by the overline) transport stream function $\overline{\psi}$, vorticity $\overline{\zeta}$ and turbulent kinetic energy $KE = \frac{1}{2}\overline{\left[(u-\bar{u})^2+(v-\bar{v})^2\right]}$ are shown in Figure 12. The time average is over 8 hours from $t = 120$ min to $t = 600$ min. For normally incident waves $\theta = 0°$, the flow develops into steady circulation cells (not shown) with a narrow offshore flow at rip channels and broad return flow in between, similar to Figure 2. This is in fact typical with moderate values of parameters H_0, ϵ, λ and μ that we explored.

[44] At a small angle of incidence $\theta = 1°$ in Figure 11, the flow becomes time dependent and somewhat irregular. The time mean flow in Figure 12 is similar to that in steady cellular circulations with $\theta = 0°$, except that the narrow rip current becomes tilted away from the normal and a weak longshore current meanders in between the cells. The turbulent kinetic energy shows that the fluctuations are predominantly localized in rip channels. At $\theta = 3°$, the irregularity in the time series is much stronger, especially along rip channels. Also as seen from the turbulent kinetic energy the spatial extent and magnitude of the fluctuations increase. Indicated by the denser contours of $\overline{\psi}$ at rip channels, the time mean rip currents are stronger and more biased in the longshore direction, but still the cellular circulation pattern is distinctive. Note that the strongest mean vorticity and local maxima in the turbulent kinetic energy are both associated with the offshore rip currents.

[45] A further increase in θ to $5°$ leads to a more pronounced longshore character in the mean flow, but the fluctuations die out after a time and the flow becomes steady eventually, see Figure 11 for $\theta = 5°$. At the steady state, the longshore velocity at a rip channel is approximately as large as the across-shore velocity. It appears that when the flow is dominated by cellular circulations a small longshore flow tends to destabilize the circulations, for example, $\theta = 1°$ and $3°$. As the longshore (noncellular) component becomes strong, it suppresses the circulation cells, and the flow starts behaving like a longshore current.

[46] At the still larger angle of $\theta = 10°$, the circulation cells have virtually disappeared. The longshore current itself becomes unstable and develops into a wave motion propagating alongshore at about $x = 100$ m. Now the turbulent kinetic energy is clearly associated with the meandering longshore currents, nearly absent from the channels. From the time series, the first and second harmonics are both present and equally strong, which may come from a period-doubling process [*Allen et al.*, 1996]. Unstable longshore currents over variable topography, with no wave-current interaction, have been studied by *Slinn et al.* [2000].

[47] From numerical experiments, we found that the spacing of rip channels also affects the instabilities of rip currents. For instance, at $\theta = 1°$ if we increase the spacing to $\lambda = 512$ m, keeping the other parameters the same, the turbulent fluctuations become more intensive. On the other hand, with a shorter spacing $\lambda = 256$ m, the flow develops into stable circulations.

[48] We have shown in section 3.2.3 that the strength of rip currents increases with ϵ. This implies that increasing ϵ has a tendency to destabilize the flow. Indeed, at $\theta = 3°$, for $\lambda = 256$ m and $\mu = 0.003$ m/s, the flow develops into steady cells with $\epsilon = 0.1$, but becomes oscillating (in time) cells with $\epsilon = 0.2$, see time series in Figure 13. Note that the oscillations are strong near the shoreline and not simple harmonic. On the other hand, we have seen in Figure 11 that the flow is strongly turbulent at $\theta = 3°$ for $\lambda = 384$ m and $\epsilon = 0.1$. Evidently, reducing the rip channel spacing tends to stabilize cellular circulations. This effect seems to be quite strong since the destabilization caused by doubling ϵ is not sufficient to overcome the effect of reducing λ from 384 m to 256 m.

3.3.2. Vorticity Evolution

[49] We now look at some details of the evolution of rip currents by examining the kinematics of vorticity. For better illustration, we choose the cases with two rip channels in the interior of the computational domain (half channel at each boundary of y).

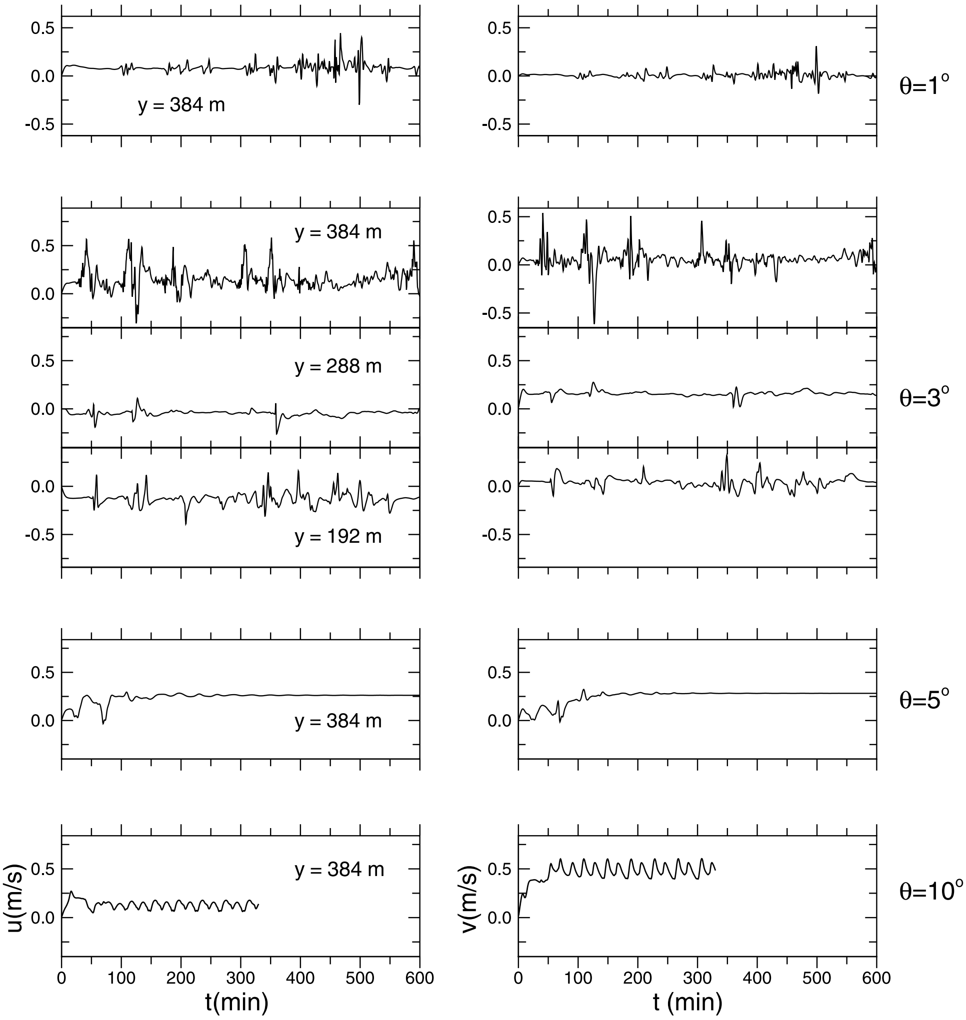

Figure 11. Time series of the u and v velocities (at x = 101 m) in a set of experiments with incidence angles θ = 1°, 3°, 5° and 10°. Wave height offshore is 1 m. μ = 0.003 m/s. ϵ = 0.1 and λ = 384 m.

[50] Figure 14 shows a sequence of vorticity fields covering one cycle of the periodic case in Figure 13. Let us focus on the patches of vorticity close to the shoreline where strong oscillations occur. During the first half cycle, the patch of negative vorticity curls up clockwise and the adjacent positive patch lengthens. In the second half cycle, this process reverses. The patches of vorticity offshore at rip channels do not appear to change their shape and position significantly, but vary somewhat in their strength.

[51] Intense temporal variations of the flow in a strong turbulent case are shown by a few snapshots of vorticity fields in Figure 15. In this case, ϵ = 0.25 and other physical parameters are the same as in Figure 13. The computational domain is L^x = 800 m and L^y = 768 m. For the convenience of description, we shall refer to the direction of increasing y as "north," as if the shoreline was along a western oceanic boundary.

[52] In the early development, the vorticity pattern is similar to that seen in the oscillatory case; compare Figure 15 at t = 40 min and Figure 14. However, the patch of positive vorticity close to the shoreline, after stretching to the north, starts ejecting vorticity at the longshore trough near x = 40 m, where rips are fed. There the flow is mainly directed toward a rip channel, and carries that vorticity into the channel, say at y = 256 m. Offshore at a rip channel ($x \simeq 100$ m), patches of positive and negative vorticity are generated, respectively, on the north and south edges of the rip channel due to waves interacting with the alongshore varying topography. The positive vorticity from close to the shore tends to form a vortex pair with the negative patch on the south edge of the channel, and migrates seaward, see t = 54 min. The positive patch on the north edge of the channel is then weakened while the seaward migrating vortex pair turns northward. When the pair joins the onshore flow over the transverse bar crest to the north, say at y = 384 m, the negative vortex of the pair has lost much of its strength, but the positive one is still strong and rejoins the positive patch on the north edge of the rip channel at y = 256 m. In the meantime, the flow generated by the migrating vortex pair, seaward and also northward, interacts with the incoming waves, producing a negative feedback to weaken the flow itself; see section 3.1. At a later time, see t = 66 min, the patch of negative vorticity close to the shoreline shoots out vorticity at the alongshore trough and into the rip channel. That forms a vortex pair with the positive patch on the north edge of the rip channel, and moves seaward while

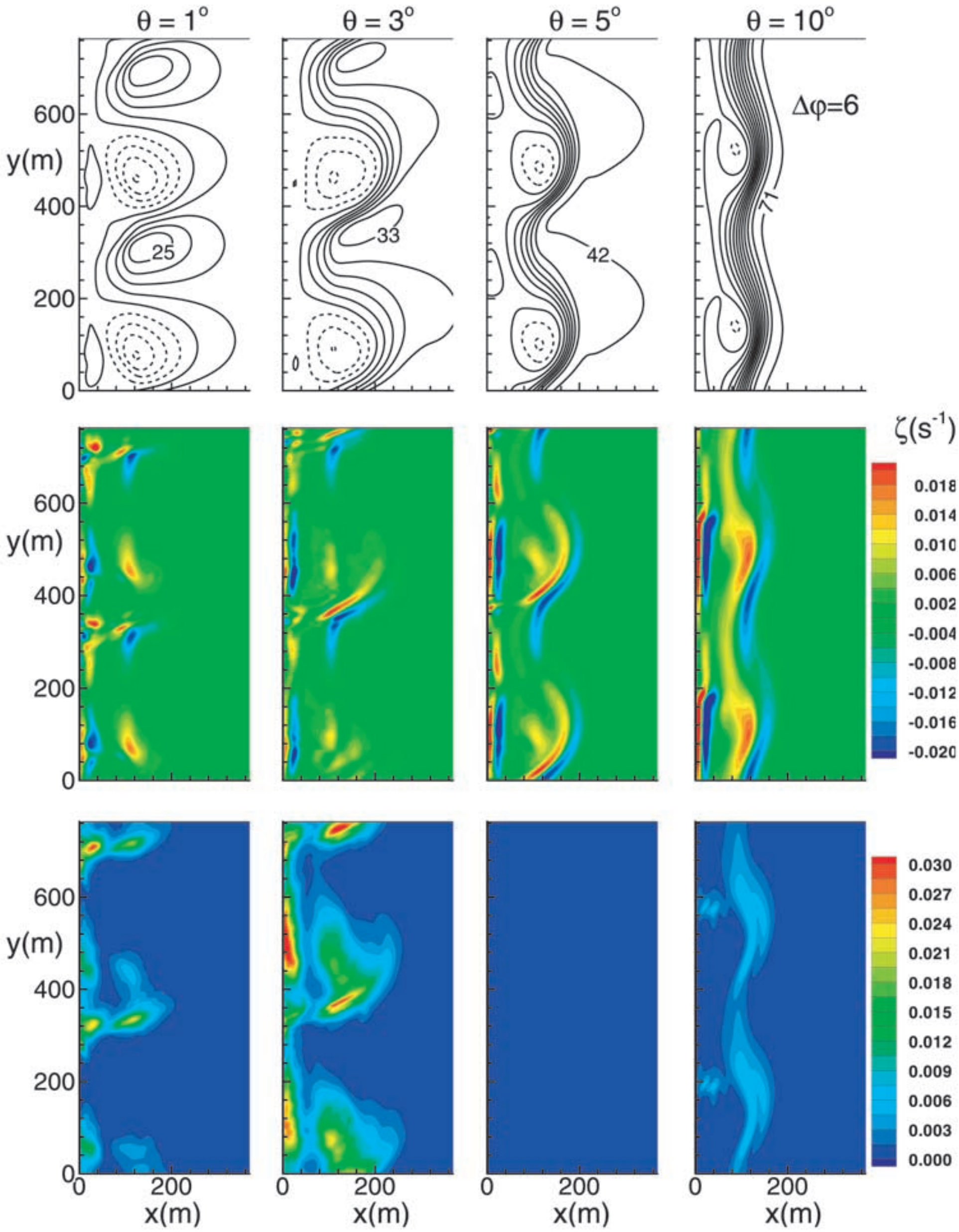

Figure 12. (top) Time mean transport stream function, (middle) vorticity field, and (bottom) turbulent kinetic energy *KE* for the experiments in Figure 11. The time average is for 8 hours from $t = 120$ min to $t = 600$ min.

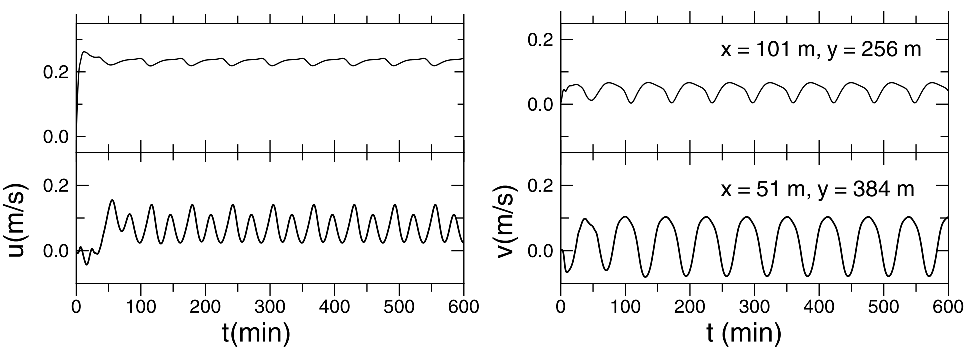

Figure 13. Time series of the u and v velocities for an oscillatory case. Parameters are $H_0 = 1$ m and $\theta = 3°$, $\mu = 0.003$ m/s, $\epsilon = 0.2$, and $\lambda = 256$ m.

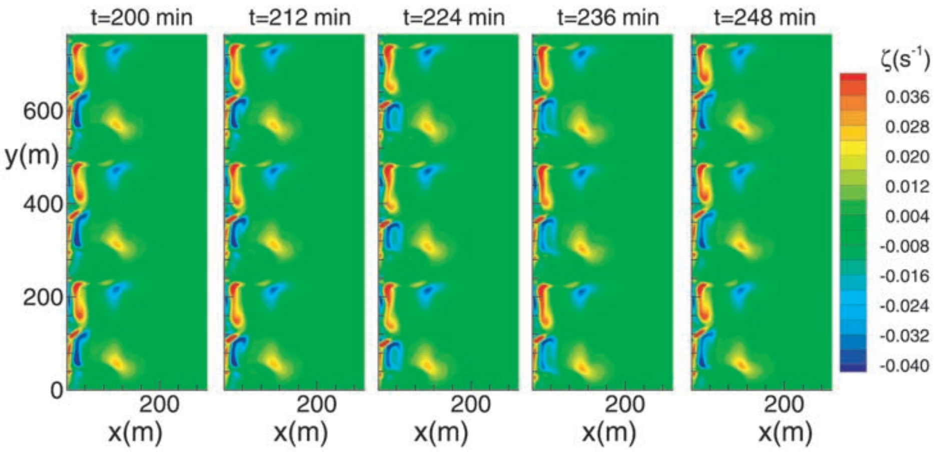

Figure 14. Snapshots of vorticity field for the oscillatory case in Figure 13.

turning south. Sometimes, all this vortex activity calms down for a while, and the pattern comes to resemble that at the early stage (e.g., $t = 40$ min). At other times, large rings of one-signed vorticity are formed close to the shore, which are irregularly shaped and rotate until the ejection of vorticity starts, see $t = 162$ min. As time goes on, the similarity of flow patterns at the different rip channels breaks down: the vorticity field can be quite active and complex at one channel, but temporarily stable at others, for instance at $t = 238$ min and $t = 285$ min. The complexity can sometimes be seen everywhere, as at $t = 390$ min.

3.3.3. Across-Shore Fluxes

[53] The offshore mass flux associated with rip currents may be used as a measurement of the strength of the currents, and may also be of interest in the study of various transport phenomena in the nearshore. We define this offshore mass flux as the alongshore average of the positive portion of the time averaged hu, and denote it as $\langle\overline{hu_+}\rangle$, where $\overline{hu_+} = \overline{hu}$ if $\overline{hu} > 0$ and is zero otherwise. Figure 16 plots the across-shore variations of $\langle\overline{hu_+}\rangle$ for the set of experiments with different incidence angles seen in Figure 12, including the steady case with $\theta = 0°$. The maxima of all the curves are located in the region 110 m $< x <$ 150 m, on the seaward face of the longshore bar, and change a little with θ. When the flow is dominated by rip current circulations, the curves are surprisingly similar, even though the flow is strongly turbulent for $\theta = 3°$ and steady for $\theta = 0°$. For large angles $\theta = 5°$ and 10°, the across-shore distribution of $\langle\overline{hu_+}\rangle$ decreases rapidly offshore, indicating that the across-shore transport of the water is much more localized for the cases of longshore currents. Note that shoreward of the maxima (at 40 m $< x <$ 120 m), the variation of $\langle\overline{hu_+}\rangle$ is practically the same in all the cases, though it is attributable to different types of flows.

[54] The time and alongshore averaged across-shore momentum flux $\langle\overline{hu^2}\rangle$ is plotted as a function of x in Figure 17 for the same experiments. For $\theta = 3°$ the most turbulent case, the across-shore momentum flux is the greatest. As θ decreases and turbulent activity becomes weaker, $\langle\overline{hu^2}\rangle$ reduces. For large angles $\theta = 5°$ and 10°, the across-shore profiles of $\langle\overline{hu^2}\rangle$ are increasingly narrow, again suggesting that the transport of the across-shore momentum is confined to the nearshore region.

4. Concluding Remarks

[55] In this study, we examined the effects of wave-current interaction on the time evolution of rip currents by using numerical experiments, which involve time integration of the two dimensional shallow water equations for currents and the wave refraction equations derived from the ray theory. Waves and currents are coupled through the wave forcing effect which is modeled using the radiation stress concept. A linear bottom friction model is utilized. Wave breaking is modeled using the simple periodic bore theory.

[56] For rip currents generated on a barred beach with gentle sinusoidal alongshore variations, several conclusions can be drawn. First, the interaction of the narrow offshore directed rip currents and incident waves produces a forcing effect opposite to that due to topography, hence it reduces the strength of the currents and restricts their offshore extent. The two physical processes due to refraction by currents, bending of wave rays and changes in the wave energy, both contribute to this negative feedback on the wave forcing. Second, the relative importance of the bottom friction, which without wave-current interaction is the only process to oppose offshore extension of rip currents, is reduced. Being largely superseded by the negative feedback arising from the interaction, changes of bottom friction parameterization do not significantly affect the predicted circulation patterns, in terms of the strength and offshore extent of the rips. This finding is particularly of importance in view of the uncertainty in the bottom friction parameterization. Third, the incident wave height has some effects on the strength and offshore extent of rip currents, but these are rather weak compared to the effects of rip channel spacing and depth. While the nonlinear convective inertia is responsible for narrowing the offshore rip currents, the width of the rip currents is ultimately determined by the width of rip channels. Finally, instabilities of the cellular circulations are sensitive to the angle of wave incidence and rip channel spacing. They develop initially at the longshore trough

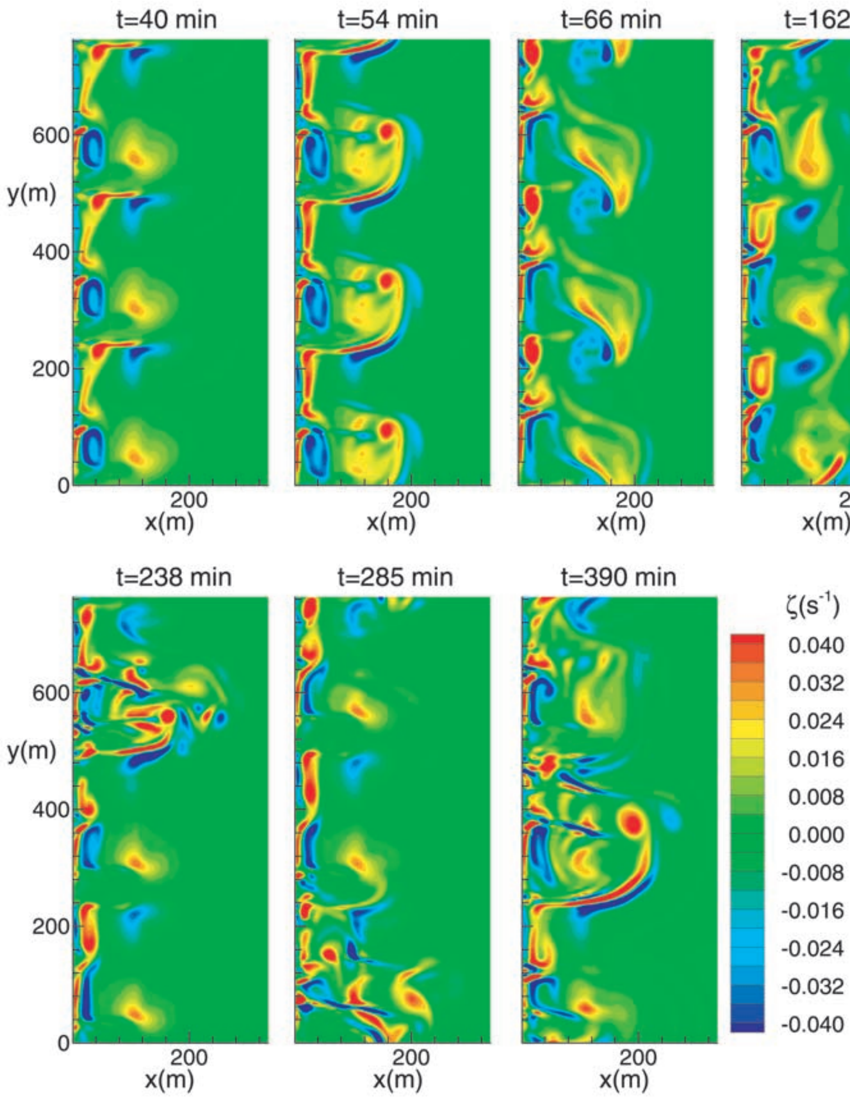

Figure 15. Snapshots of vorticity field for a strong turbulent case. Parameters are H_0 = 1 m, $\theta = 3°$, μ = 0.003 m/s, ϵ = 0.25 and λ = 256 m.

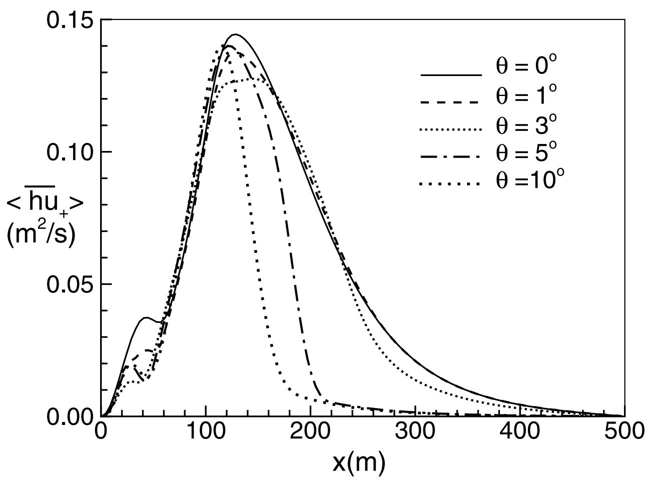

Figure 16. Time-averaged offshore mass flux due to rip currents for the experiments in Figure 11.

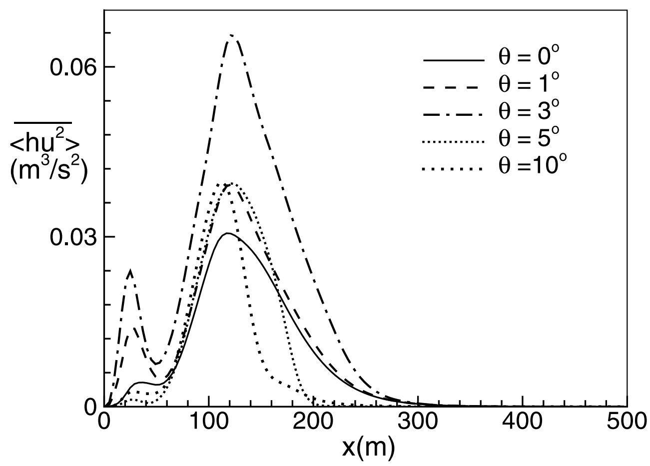

Figure 17. Time- and alongshore-averaged across-shore momentum flux for the experiments in Figure 11.

where rips are fed, rather than offshore at rip heads as predicted with no interaction. Vortex shedding and pairing are associated with the turbulent rip currents. The time mean flows nevertheless are still similar to those in steady cases.

5. Further Comments

[57] With regard to the large scale features, the present model seems able to give a qualitatively reasonable description of nearshore cellular circulations. The model of course is not intended for quantitative predictions on real beaches. For that purpose various other phenomena would also have to be considered, such as: (1) lateral momentum mixing due to turbulence and/or dispersion effects associated with vertical variations in currents [*Svendsen and Putrevu*, 1994]; (2) a more realistic bottom friction model, for instance a nonlinear across-shore varying version; (3) possible occurrence of ray crossing, caustics, wave blocking by opposing currents faster than the wave propagation speed, flow or topographic scales comparable to the wavelength: all things requiring extensions of the simple ray theory and the inclusion of diffractive effects. Some of these singular cases are discussed by *Mei* [1989] and *Kirby* [1988], among others.

[58] While these difficult matters are not so essential for our main purpose of emphasizing the importance of wave-current interaction in models of topographically driven rip currents, there are also certain limitations to our treatment which should be appreciated. Overcoming these limitations seems to call for basic improvements in our fundamental understanding. First, the wave radiation stress formula [*Longuet-Higgins and Stewart*, 1964] has been used to model the momentum transfer to currents, as in most studies of nearshore currents for the past thirty years. This formula was derived based on small amplitude waves in irrotational flows. Its use in the surf zone lacks justification, though it has produced reasonable results on plane beaches. Some suggestions for improving the modeling of wave forcing have been proposed, for instance inclusion of surface rollers (another model of wave breaking). Recently, *Bühler and Jacobson* [2001, and personal communication, 2000] suggested that direct application of *Longuet-Higgins and Stewart* [1964] to the cases of longshore inhomogeneity is not adequate because of the strong vorticity which may be produced by breaking waves and strong currents, and put forward an adaptation of it based on the pseudo-momentum concept [*Bühler*, 2000; *Andrews and McIntyre*, 1978]. Second, the wave dissipation function ϵ_b adopted here (and those in other studies using similar models) was developed for the cases of longshore uniformity. Its suitability for longshore inhomogeneity, whether caused by topography, by currents, or by the incident waves, has not been carefully studied.

Appendix A: Bottom Topography

[59] The beach profile measured at Duck, North Carolina, on October 11, 1990, is approximated as

$$h_0(x) = (a_1 - a_1/\gamma_1)\tanh\left(\frac{b_1 x}{a_1}\right) + \frac{b_1 x}{\gamma_1} - a_2 \exp\left[-5\left(\frac{x - x_c}{x_c}\right)^2\right], \quad \text{(A1)}$$

where $x_c = 80$ m is the location of the longshore bar and $\gamma_1 = \tan\beta_1/\tan\beta_2$ with $\beta_1 = 0.075$ being the beach slope close to the shore and $\beta_2 = 0.0064$ the slope offshore of the bar. $b_1 = \tan\beta_1$, $a_1 = 2.97$ m and $a_2 = 1.5$ m. A sinusoidal longshore perturbation is added at the longshore bar and the perturbed bottom profile is:

$$h(x,y) = h_0(x) + h_0(x)\epsilon\cos\left(\frac{2\pi y}{\lambda}\right)\exp\left[-5\left(\frac{x - x_c}{x_c}\right)^2\right]. \quad \text{(A2)}$$

Here ϵ is the magnitude of the perturbation and measures the depth of rip channels. λ is the wavelength of the perturbation (or spacing of rip channels).

[60] **Acknowledgments.** This research is supported by the Office of Naval Research (ONR) Coastal Dynamics Program through the Young Investigator Program under grant N00014-99-1-0489. JY gratefully acknowledges the many stimulating discussions with Louis N. Howard. During the time of revision, JY was supported by Andrew W. Mellon Foundation through a grant to A. Brad Murray at Duke University.

References

Allen, J. S., P. A. Newberger, and R. A. Holman, Nonlinear shear instabilities of alongshore currents on plane beaches, *J. Fluid Mech.*, *310*, 181–213, 1996.

Andrews, D. G., and M. E. McIntyre, An exact theory of nonlinear waves on a Lagrangian-mean flow, *J. Fluid Mech.*, *89*, 609–646, 1978.

Arthur, R. S., Refraction of shallow water waves: The combined effect of currents and underwater topography, *Eos Trans. AGU*, *31*, 549–552, 1950.

Arthur, R. S., A note on the dynamics of rip currents, *J. Geophys. Res.*, *67*, 2777–2779, 1962.

Bowen, A. J., The generation of longshore currents on a plane beach, *J. Mar. Res.*, *27*, 206–215, 1969a.

Bowen, A. J., Rip currents, 1, Theoretical investigations, *J. Geophys. Res.*, *74*, 5467–5478, 1969b.

Bowen, A. J., and D. L. Inman, Rip currents, 2, Laboratory and field observations, *J. Geophys. Res.*, *74*, 5479–5490, 1969.

Bühler, O., On the vorticity transport due to dissipating or breaking waves in shallow-water flow, *J. Fluid Mech.*, *407*, 235–263, 2000.

Bühler, O., and T. E. Jacobson, Wave-driven currents and vortex dynamics on barred beaches, *J. Fluid. Mech.*, *449*, 331–339, 2001.

Chen, Q., R. A. Dalrymple, J. T. Kirby, A. B. Kennedy, and M. C. Haller, Boussinesq modeling of a rip current system, *J. Geophys. Res.*, *104*, 20,617–20,637, 1999.

Church, J. C., and E. B. Thornton, Effects of breaking wave induced turbulence within a longshore current model, *Coastal Eng.*, *20*, 1–28, 1993.

Cooke, D. O., The occurrence and geological work of rip currents off southern California, *Mar. Geol.*, *9*, 173–186, 1970.

Dalrymple, R. A., A mechanism of rip current generation on an open coast, *J. Geophys. Res.*, *80*, 3485–3487, 1975.

Dalrymple, R. A., and C. T. Lozano, Wave-current interaction models for rip currents, *J. Geophys. Res.*, *83*, 6063–6071, 1978.

Dodd, N., On the destabilization of a longshore current on a plane beach: Bottom shear stress, critical conditions and onset of instabilities, *J. Geophys. Res.*, *99*, 811–824, 1994.

Falqués, A., A. Montoto, and D. Vila, A note on hydrodynamic instabilities and horizontal circulations in the surf zone, *J. Geophys. Res.*, *104*, 20,605–20,615, 1999.

Haas, K. A., I. A. Svendsen, and M. C. Haller, Numerical modeling of nearshore circulations on a barred beach with rip channels, paper presented at 26th Conference on Coastal Engineering, Am. Soc. of Civ. Eng., Copenhagen, Den., 1998.

Haller, M. C., R. A. Dalrymple, and I. A. Svendsen, Experimental modeling of a rip current system, paper presented at Proceedings of Ocean Wave Measurement and Analysis, Waves'97, Am. Soc. of Civ. Eng., Va. Beach, Va., 1997.

Harris, T. F. W., The nearshore circulation of water, paper presented at CSIR Symposium S2, Counc. for Sci and Ind. Res., South Africa, 1961.

Harris, T. F. W., A qualitative study of the nearshore circulation off a Natal beach with a submerged longshore sand bar, M. S. thesis, Univ. of Natal, Durban, South Africa, 1964.

Harris, T. F. W., Field and model studies of the nearshore circulation, Ph.D diss., Univ. of Natal, Durban, South Africa, 1967.

Hino, M., Theory on formation of rip-current and cuspidal coast, paper presented at 14th Conference on Coastal Engineering, Am. Soc. of Civ. Eng., Copenhagen, Den., 1974.

Hunter, R. E., H. E. Clifton, and R. L. Phillips, Depositional processes, sedimentary structures, and predicted vertical sequences in barred nearshore system, southern Oregon coast, *J. Sediment. Petrol.*, *49*, 711–726, 1979.

Kirby, J. T., Discussion of "Refraction-diffraction model for linear water waves" by B. A. Ebersole, *J. Waterw. Port Coastal Ocean Eng.*, *114*, 101–103, 1988.

LeBlond, P. H., and C. L. Tang, On energy coupling between waves and rip currents, *J. Geophys. Res.*, *79*, 811–816, 1974.

Lippmann, T. C., A. H. Brookins, and E. B. Thornton, Wave energy transformation on natural profiles, *Coastal Eng.*, *27*, 1–20, 1996.

Lippmann, T. C., H. C. Herbers, and E. B. Thornton, Gravity and shear wave contributions to nearshore infragravity motions, *J. Phys. Oceanogr.*, *29*, 231–239, 1999.

Liu, P. L.-F., and C. C. Mei, Water motion on a beach in the presence of a breakwater, 2, Mean currents, *J. Geophys. Res.*, *81*, 3085–3094, 1976.

Longuet-Higgins, M. S., Mass transport in water waves, *Philos. Trans. R. Soc., London, Ser. A*, *245*, 535–581, 1953.

Longuet-Higgins, M. S., Longshore currents generated by obliquely incident sea waves, 2, *J. Geophys. Res.*, *75*, 6790–6801, 1970.

Longuet-Higgins, M. S., and R. W. Stewart, The changes in the form of short gravity waves on long waves and tidal currents, *J. Fluid Mech.*, *8*, 565–583, 1960.

Longuet-Higgins, M. S., and R. W. Stewart, The changes in amplitude of short gravity waves on steady non-uniform currents, *J. Fluid Mech.*, *10*, 529–549, 1961.

Longuet-Higgins, M. S., and R. W. Stewart, Radiation stress and mass transport in gravity waves, with application to "surf-beats", *J. Fluid Mech.*, *13*, 481–504, 1962.

Longuet-Higgins, M. S., and R. W. Stewart, Radiation stress in water waves: A physical discussion, with applications, *Deep Sea Res.*, *11*, 529–562, 1964.

McKenzie, R., Rip current system, *J. Geol.*, *66*, 103–113, 1958.

Mei, C. C., *The Applied Dynamics of Ocean Surface Waves*, World Sci, River Edge, N.J., 1989.

Miller, C., and A. Barcilon, Hydrodynamic instability in the surf zone as a mechanism for the formation of gyres, *J. Geophys. Res.*, *83*, 4107–4116, 1978.

Noda, E. K., Wave-induced nearshore circulation, J, *Geophys. Res.*, *79*, 4097–4106, 1974.

Özkan-Haller, H. T., and J. T. Kirby, Nonlinear evolution of shear instabilities of the longshore current: A comparison of observations and computations, *J. Geophys. Res.*, *104*, 25,953–25,984, 1999.

Sasaki, T. O., and K. Horikawa, Observations of nearshore current and edge waves, paper presented at 16th Coastal Engineering Conference, Am. Soc. of Civ. Eng., Hamburg, Germany, 1979.

Shepard, F. P., and D. L. Inman, Nearshore circulation related to bottom topography and wave refraction, *Eos Trans. AGU*, *31*(4), 555–565, 1950.

Shepard, F. P., and D. L. Inman, Nearshore circulation, paper presented at 1st Conference on Coastal Engineering, Counc. on Wave Res., Univ. of Calif., Long Beach, 1951.

Shepard, F. P., K. O. Emery, and E. C. LaFond, Rip currents: A process of geological importance, *J. Geol.*, *49*, 337–369, 1941.

Short, A. D., Beach and nearshore facies: Southeast Australia, in *Hydrodynamics and Sedimentation in Wave-Dominated Coastal Environments*, edited by B. Greenwood and R. A. Davies Jr., *Mar. Geol., 60*, 261–282, 1984.

Short, A. D., Rip-current type, spacing and persistence, Narrabeen beach, Australia, *Mar. Geol.*, *65*, 47–71, 1985.

Slinn, D. N., J. S. Allen, P. A. Newberger, and R. A. Holman, Nonlinear shear instabilities of alongshore currents over barred beaches, *J. Geophys. Res.*, *103*, 18,357–18,379, 1998.

Slinn, D. N., J. S. Allen, and R. A. Holman, Alongshore currents over variable beach topography, *J. Geophys. Res.*, *105*, 16,971–16,998, 2000.

Smith, J. A., and J. L. Largier, Observations of nearshore circulation: Rip currents, *J. Geophys. Res.*, *100*, 10,967–10,975, 1995.

Sonu, C. J., Field observations of nearshore circulation and meandering currents, *J. Geophys. Res.*, *77*, 3232–3247, 1972.

Stoker, J. J., *Water Waves*, Wiley-Interscience, New York, 1957.

Svendsen, I. A., and U. Putrevu, Nearshore mixing and dispersion, *Proc. R. Soc., London, Ser. A*, *445*, 561–576, 1994.

Thornton, E. B., Variation of longshore current across the surf zone, paper persented at 12th Coastal Engineering Conference, Am. Soc. of Civ. Eng., Washington, D. C., 1970.

Thornton, E. B., and R. T. Guza, Transformation of wave height distribution, *J. Geophys. Res.*, *88*, 5929–5938, 1983.

Thornton, E. B., and R. T. Guza, Surf zone longshore currents and random waves: Field data and models, *J. Phys. Oceanogr.*, *16*, 1165–1178, 1986.

Wei, G., J. T. Kirby, S. T. Grilli, and R. Subramanya, A fully nonlinear Boussinesq model for surface waves, 1, Highly nonlinear unsteady waves, *J. Fluid Mech.*, *294*, 71–92, 1995.

Whitham, G. B., *Linear and Nonlinear Waves*, Wiley-Interscience, New York, 1974.

D. N. Slinn, Department of Civil and Coastal Engineering, University of Florida, Gainesville, FL 32611-6580, USA. (slinn@coastal.ufl.edu)

J. Yu, Division of Earth and Ocean Sciences, Duke University, Box 90227, Durham, NC 27708, USA. (jyu@duke.edu)